RadioGraphics

Differential Diagnosis for Bilateral Abnormalities of the Basal Ganglia and Thalamus[1]

Amogh N. Hegde, MD, FRCR • Suyash Mohan, MD, PDCC
Narayan Lath, MD, FRCR • C. C. Tchoyoson Lim, MMed, FRCR

CME FEATURE

See www.rsna.org/education/rg_cme.html

LEARNING OBJECTIVES FOR TEST 1

After reading this article and taking the test, the reader will be able to:

- List the conditions that manifest as bilateral involvement of the basal ganglia and thalamus.
- Describe the clinical, laboratory, and imaging features of these conditions.
- Discuss the clinical and radiologic differential diagnoses for these conditions.

TEACHING POINTS

See last page

The basal ganglia and thalamus are paired deep gray matter structures that may be involved by a wide variety of disease entities. The basal ganglia are highly metabolically active and are symmetrically affected in toxic poisoning, metabolic abnormalities, and neurodegeneration with brain iron accumulation. Both the basal ganglia and thalamus may be affected by other systemic or metabolic disease, degenerative disease, and vascular conditions. Focal flavivirus infections, toxoplasmosis, and primary central nervous system lymphoma may also involve both deep gray matter structures. The thalamus is more typically affected alone by focal conditions than by systemic disease. Radiologists may detect bilateral abnormalities of the basal ganglia and thalamus in different acute and chronic clinical situations, and although magnetic resonance (MR) imaging is the modality of choice for evaluation, the correct diagnosis can be made only by taking all relevant clinical and laboratory information into account. The neuroimaging diagnosis is influenced not only by detection of specific MR imaging features such as restricted diffusion and the presence of hemorrhage, but also by detection of abnormalities involving other parts of the brain, especially the cerebral cortex, brainstem, and white matter. Judicious use of confirmatory neuroimaging investigations, especially diffusion-weighted imaging, MR angiography, MR venography, and MR spectroscopy during the same examination, may help improve characterization of these abnormalities and help narrow the differential diagnosis.

Abbreviations: AIDS = acquired immunodeficiency syndrome, CJD = Creutzfeldt-Jakob disease, CNS = central nervous system, CSF = cerebrospinal fluid, CVT = cerebral venous thrombosis, HIE = hypoxic ischemic encephalopathy, HIV = human immunodeficiency virus, NBIA = neurodegeneration with brain iron accumulation, PBTG = primary bilateral thalamic glioma

RadioGraphics 2011; 31:5–30 • **Published online** 10.1148/rg.311105041 • **Content Codes:** MR NR

[1]From the Department of Neuroradiology, National Neuroscience Institute, Singapore (A.N.H., C.C.T.L.); Department of Diagnostic Radiology, Singapore General Hospital, Block 4, Level 1, Outram Rd, Singapore 169608 (A.N.H., N.L.); Neuroradiology Division, Department of Radiology, University of Michigan Health System, Ann Arbor, Mich (S.M.); and Department of Diagnostic Imaging, Yong Loo Lin School of Medicine, National University of Singapore, Singapore (C.C.T.L.). Recipient of a Certificate of Merit award for an education exhibit at the 2009 RSNA Annual Meeting. Received March 3, 2010; revision requested March 29; final revision received May 21; accepted May 25. For this CME activity, the authors, editors, and reviewers have no relevant relationships to disclose. **Address correspondence to** A.N.H. (e-mail: *amogh77@yahoo.co.in*).

Introduction

Abnormalities of the basal ganglia and thalamus may be detected at neuroimaging in a wide variety of pathologic conditions. The causes of these abnormalities may be broadly classified as systemic or focal, some with acute onset and others with slowly progressive manifestations. The deep gray matter nuclei may be affected by toxic poisoning (by carbon monoxide, methanol, cyanide) and systemic metabolic abnormalities (eg, liver disease, hyper- or hypoglycemia, hypoxia, Leigh disease, Wilson disease, osmotic myelinolysis, Wernicke encephalopathy). Certain degenerative conditions (eg, Huntington disease, neurodegeneration with brain iron accumulation [NBIA], Creutzfeldt-Jakob disease [CJD], Fahr disease) and vascular abnormalities (venous infarction, arterial occlusion) also have a predilection for involving the basal ganglia and thalamus. Finally, some focal inflammatory and infectious conditions (neuro-Behçet disease, flavivirus encephalitides, toxoplasmosis) or neoplasms (primary central nervous system [CNS] lymphoma, primary bilateral thalamic glioma [PBTG]) may also affect the basal ganglia and thalamus on both sides.

Although magnetic resonance (MR) imaging is the modality of choice for evaluating the basal ganglia, computed tomography (CT) may be the first line of investigation, particularly in emergency situations in which patients present with altered sensorium or acute-onset seizures. There is considerable variation and overlap in both the clinical and radiologic features of abnormalities affecting the deep gray matter nuclei. Hence, no classification scheme is foolproof, and radiologists can contribute greatly to the correct diagnosis by correlating the imaging features with available clinical and laboratory data.

In this article, we review the MR imaging anatomy of the basal ganglia and thalamus, discuss and illustrate a wide variety of pathologic conditions of these brain structures, and discuss the radiologic assessment of these conditions.

MR Imaging Anatomy of the Basal Ganglia and Thalamus

The deep gray matter nuclei include the basal ganglia and thalamus, paired structures that are situated at the base of the forebrain and have wide connections to the cortex and other parts of the brain. Although some anatomists consider the subthalamic nucleus and substantia nigra to be part of the basal ganglia and the classification of terms is somewhat controversial (1), in this article we restrict our discussion to abnormalities of the lentiform and caudate nuclei. On axial brain images, the lentiform nucleus and the head of the caudate nucleus can be visualized as paired symmetric structures located between the lateral ventricle and the insular cortex (Fig 1). The lentiform nucleus, which includes the putamen and the more medially located globus pallidus, is separated from the caudate head and the thalamus by the anterior and posterior limbs of the internal capsule, respectively. At MR imaging, the caudate nucleus and putamen are isointense relative to the cortical gray matter with all pulse sequences and do not enhance after contrast material injection. The globus pallidus is typically slightly hypointense relative to the putamen, a normal feature that is attributable to progressive iron deposition as one ages (1). The lentiform nucleus can also exhibit dilated Virchow-Robin perivascular spaces (Fig 2a) and bilaterally symmetric age-related calcification (Fig 2b), both of which are considered normal findings and should not be confused with pathologic changes (2,3).

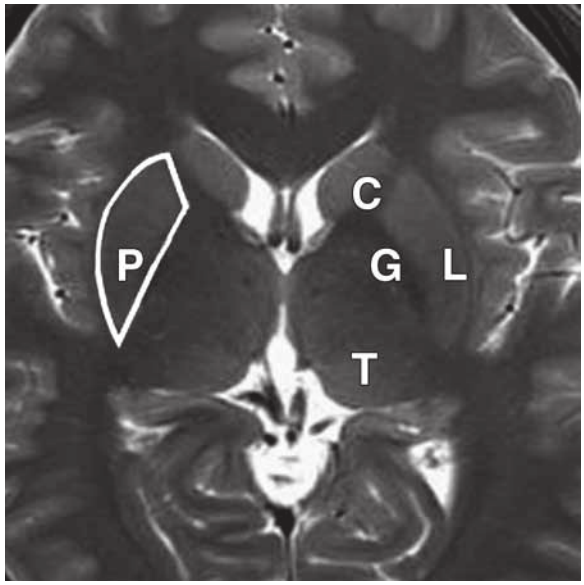

Figure 1. Axial T2-weighted MR image shows the normal anatomy of the deep gray matter structures. *C* = caudate nucleus, *G* = globus pallidus, *L* = lentiform nucleus, *P* = putamen, *T* = thalamus.

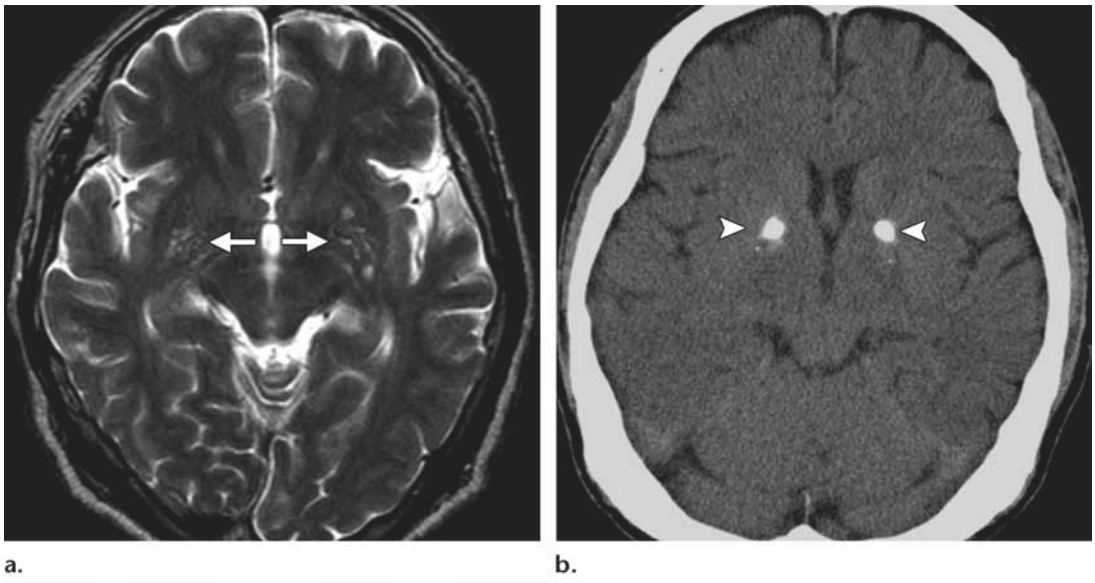

Figure 2. Spectrum of normal imaging appearances of the basal ganglia. **(a)** Axial T2-weighted MR image shows well-defined rounded foci (arrows) that are isointense relative to the cerebrospinal fluid (CSF), findings that represent prominent Virchow-Robin (perivascular) spaces. **(b)** CT scan obtained without the use of contrast material demonstrates bilateral physiologic calcification (arrowheads) in the basal ganglia. **(c)** Axial gradient-recalled echo image clearly depicts physiologic iron deposition in the globus pallidus (arrowheads) as symmetric hypointense areas.

Teaching Point

The functions of the basal ganglia are complex. These structures are mainly involved in the production of movement and are a part of the extrapyramidal motor system, but they may also be involved in memory, emotion, and other cognitive functions (4). The putamen and globus pallidus are rich in mitochondria, vascular supply, neurotransmitters, and chemical content compared with other areas in the brain, and their high metabolic activity and increased utilization of glucose and oxygen make them vulnerable to metabolic abnormalities and many systemic or generalized disease processes (5). Hence, when the basal ganglia are seen to be affected at MR imaging, the clinical signs and symptoms can vary from movement disorders (eg, chorea, tremors, bradykinesia, dystonia) to coma, depending on whether there is focal involvement of the basal ganglia in isolation or generalized metabolic derangement with widespread brain necrosis.

The thalamus is a midline structure situated between the cerebral hemispheres and the midbrain, with paired symmetric portions located on either side of the third ventricles (Fig 1). It consists of multiple nuclei that are responsible for relaying sensory and motor signals to and from the cerebral cortex and are involved in regulating consciousness, sleep, and alertness. Hence, lesions affecting the thalamus often result in disorders of consciousness and abnormalities of sensation (6).

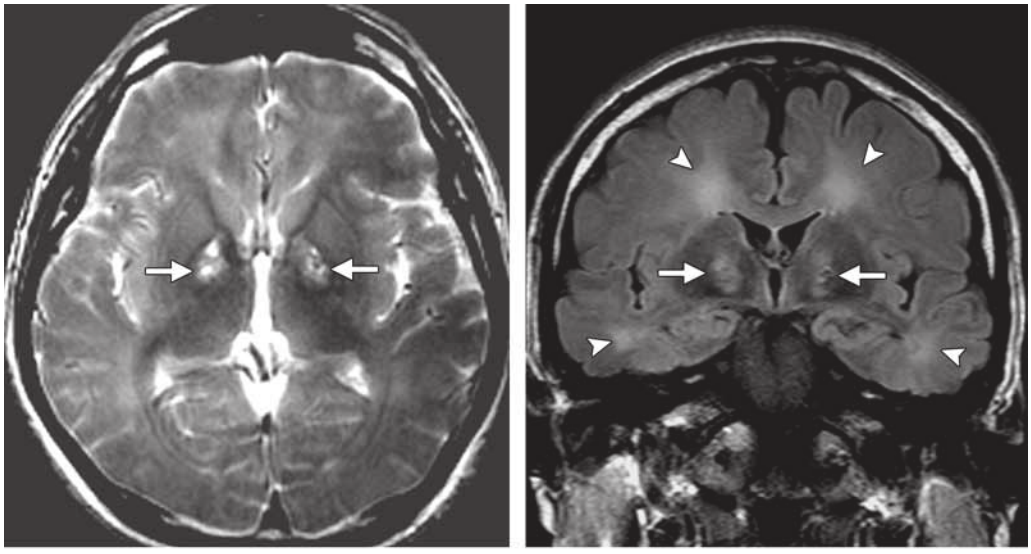

a. b.

Figure 3. Carbon monoxide poisoning in a 33-year-old man who was found in a coma after a suicide attempt. Axial T2-weighted **(a)** and coronal fluid-attenuated inversion recovery **(b)** MR images obtained 4 weeks after the poisoning depict symmetric hyperintense foci in the globus pallidus (arrows). Symmetric hyperintense areas in the deep white matter (arrowheads in **b**) are consistent with delayed leukoencephalopathy.

Radiologists should be familiar with the arterial supply and venous drainage of the deep gray matter nuclei because there are significant implications. The basal ganglia derive their blood supply from the medial and lateral lenticulostriate arteries, which arise from the anterior and middle cerebral arteries, respectively (7). On the other hand, the thalamus derives its arterial supply from the first and second parts of the posterior cerebral artery, with contributions from the posterior communicating artery (6). There is considerable variation in the arterial supply of the thalamus in healthy individuals, and radiologists should be aware of the patterns of thalamic infarction (see "Arterial Occlusion"). Venous drainage of both the basal ganglia and the thalamus is into the deep (rather than superficial) venous system (8); this has implications in venous thrombosis and infarction (see "Deep Venous Sinus Thrombosis"). The superior and inferior thalamostriate veins, along with several smaller surface veins, drain into the paired internal cerebral veins. These join the basal vein of Rosenthal to form the great vein of Galen at a point inferior to the splenium of the corpus callosum, where the great vein of Galen joins the inferior sagittal sinus to form the straight sinus. The straight sinus then continues backward to the torcula and joins the superficial dural venous sinus system (8).

Pathologic Conditions of the Basal Ganglia and Thalamus

Toxic Poisoning

Carbon monoxide, methanol, and cyanide are cellular respiratory toxins that affect the mitochondria (9,10). Carbon monoxide inhibits electron transport (11), methanol is metabolized to toxic formate, and cyanide blocks trivalent iron in the cellular respiratory chain; in all three scenarios, the result is impairment of mitochondrial cellular respiratory enzymes. Patients usually present with acute cognitive impairment or coma after accidental exposure or attempted suicide. Methanol poisoning in particular may manifest with optic neuritis as its initial symptom. The diagnosis is usually established with appropriate toxicologic and laboratory tests, with imaging being used to assess brain damage.

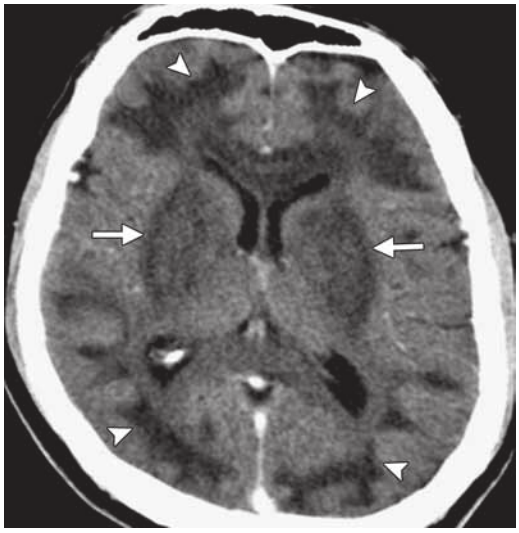

Figure 4. Methanol poisoning in a 41-year-old man who presented with altered mental status and retrobulbar pain. Contrast material–enhanced CT scan demonstrates hypoattenuating areas in the lentiform nuclei (arrows), corpus callosum, and subcortical deep white matter in the frontal and parieto-occipital regions (arrowheads). (Courtesy of Anirudh Kohli, MD, Breach Candy Hospital Trust, Mumbai, India.)

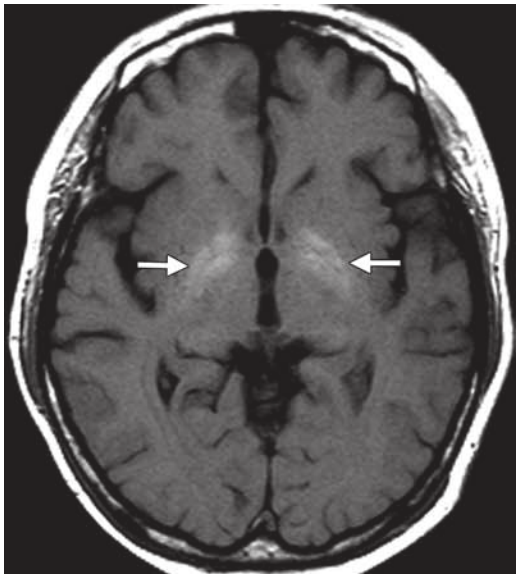

Figure 5. Hepatic cirrhosis in a 55-year-old man. T1-weighted MR image depicts symmetric hyperintense foci in the globus pallidus (arrows).

Because of their high metabolic activity, respiratory toxins tend to cause bilateral MR imaging abnormalities in the basal ganglia, sometimes with diffuse involvement of other brain structures (9). Carbon monoxide in particular has a propensity to affect the globus pallidus (Fig 3) (11). T2 prolongation in the basal ganglia is typical in acute poisoning, often with restricted diffusion on diffusion-weighted MR images. In carbon monoxide poisoning, delayed leukoencephalopathy (Fig 3b) and T1 shortening in the globus pallidus may be encountered (11). Hemorrhagic necrosis of the putamen may be observed in cyanide and methanol poisoning, and white matter edema may be an additional feature of methanol poisoning (Fig 4) (9).

Liver Disease

The basal ganglia may be affected in patients with liver dysfunction. Most patients have a history of chronic cirrhosis with portal hypertension and iatrogenic (ie, placed with transjugular intrahepatic portosystemic shunt surgery) or spontaneous portosystemic shunts, resulting in nitrogenous waste products crossing the blood-brain barrier and causing long-term toxic brain damage.

Brain MR imaging findings in hepatic cirrhosis include bilateral hyperintense areas in the globus pallidus and substantia nigra on T1-weighted images (Fig 5). These findings have been attributed to the deposition of manganese (12) and may be reversible after liver transplantation (13). Characteristic MR imaging signs of acute brain damage may be present in patients with acute hyperammonemia, including cirrhotic patients with acute hepatic decompensation (in whom the ammonia concentration can suddenly increase fourfold) and patients with ornithine transcarbamylase deficiency (ie, inborn errors of metabolism such

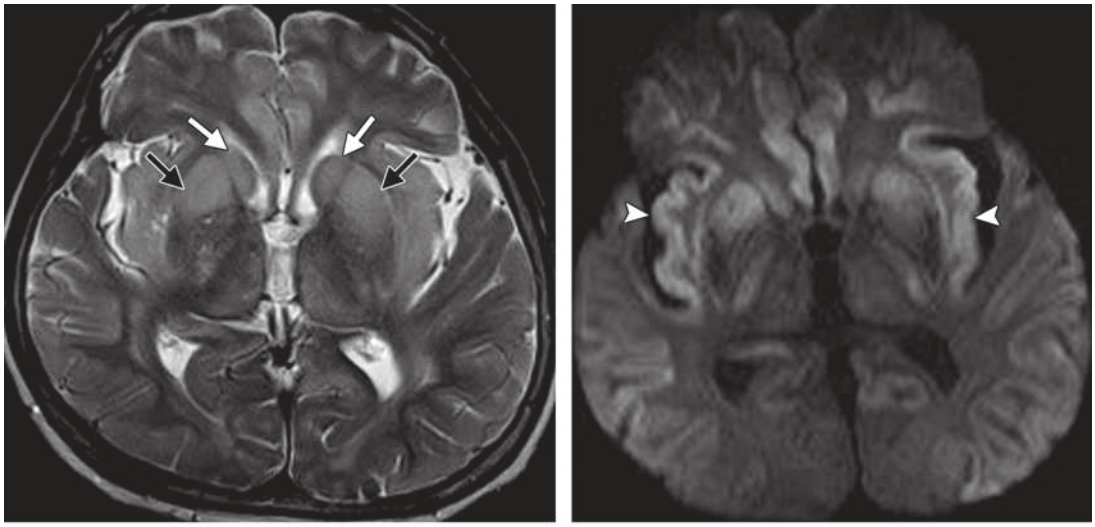

a. b.

Figure 6. Acute hyperammonemia in a 70-year-old cirrhotic man with acute decompensated hepatic failure who presented with altered mental status. T2-weighted **(a)** and diffusion-weighted **(b)** MR images reveal bilaterally symmetric swelling, hyperintensity, and restricted diffusion in the caudate heads (white arrows in **a**), putamina (black arrows in **a**), and insular cortices (arrowheads in **b**).

as citrullinemia, which result in accumulation of ammonia in the brain) (14). Acute hyperammonemia causes bilaterally symmetric swelling, T2 prolongation, and restricted diffusion in the basal ganglia, insular cortex, and cingulate gyrus (Fig 6) (15,16). MR spectroscopic detection of the combined toxic metabolite glutamate-glutamine at short echo times in the acutely affected brain has been described (14).

Nonketotic Hyperglycemia

Patients with hyperglycemia are typically individuals with poorly controlled diabetes who present with acute chorea, hemiballismus, and, sometimes, altered mental status. Hyperglycemia is a treatable condition with a good prognosis, and follow-up neuroimaging performed 2–12 months later usually shows the resolution of findings (17).

CT typically shows bilateral or, rarely, unilateral pallidal or caudate hyperattenuation. At MR imaging, the abnormal areas are characteristically hyperintense on T1-weighted images (Fig 7) and of variable intensity on T2-weighted images (17,18). The mechanism for signal abnormalities is unknown, and various hypotheses involving the deposition of proteins, myelin breakdown products, blood, or calcium or other minerals have been proposed. Besides hyperglycemia, other important causes of bilateral pallidal T1 shortening include manganese deposition in hepatic encephalopathy (discussed earlier), chronic occupational exposure to manganese, and long-term treatment with total parenteral nutrition.

Hypoglycemia

Patients who present with hypoglycemic coma are typically diabetic patients who accidentally overdose while receiving treatment with oral hypoglycemic agents (typically the long-acting sulfonylurea group of drugs) (19). Rarely, nondiabetic patients can present with unexplained hypoglycemia; in such cases, undiagnosed insulinoma of the pancreas or the occult effects of medications with hypoglycemic effects (including alternative or "herbal" preparations) should be considered (20,21). The extent of brain damage depends on the severity and duration of hypoglycemia, and clinical presentation includes seizures, focal neurologic deficits, and coma.

Characteristic MR imaging findings of severe hypoglycemia include bilateral T2 prolongation in the cerebral cortex, hippocampi, and basal ganglia (Fig 8a) (22). In some cases of milder, reversible hypoglycemia, transient and isolated white matter abnormalities involving the splenium of the corpus callosum, internal capsules, and corona

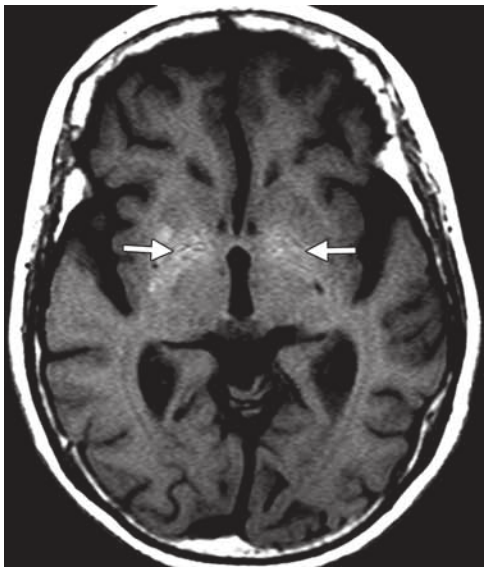

Figure 7. Nonketotic hyperglycemia in a 68-year-old woman with uncontrolled diabetes and choreoathetoid movements. Axial T1-weighted MR image reveals bilateral hyperintense pallidal areas (arrows).

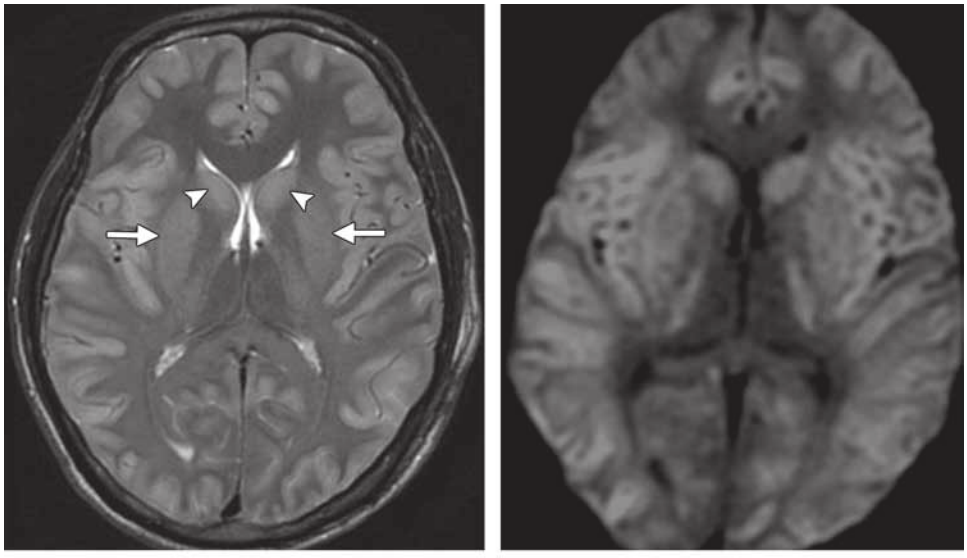

a. b.

Figure 8. Hypoglycemic brain injury in an 18-year-old comatose man with a random blood sugar level of 2.1 mmol/L. Axial T2-weighted **(a)** and diffusion-weighted **(b)** MR images demonstrate diffuse hyperintensity and restricted diffusion in the heads of the caudate nuclei (arrowheads in **a**), lentiform nuclei (arrows in **a**), and cerebral cortex, with sparing of the subcortical white matter and thalamus.

radiata have been reported, with patients making a full recovery without neurologic deficit; however, white matter lesions may also be seen in combination with severe, diffuse gray matter abnormalities (21,23). The abnormal areas are typically hyperintense on diffusion-weighted MR images (Fig 8b) and show a reduced apparent diffusion coefficient (24). Involvement of the basal ganglia seems to portend a poor prognosis (22). In patients with unexplained coma, determination of blood serum sugar levels can help differentiate this potentially reversible condition from other causes such as hypoxic ischemic encephalopathy (HIE) or acute cerebral infarction (23).

Teaching Point

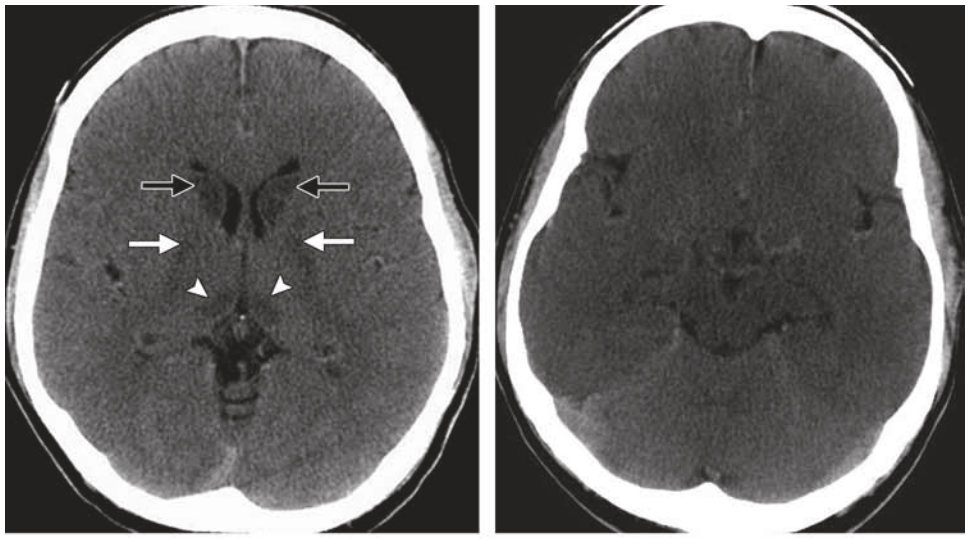

a. b.

Figure 9. HIE in a 54-year-old man who was resuscitated after experiencing cardiac arrest. **(a)** Noncontrast CT scan reveals bilaterally symmetric hypoattenuating areas in the thalamus (arrowheads), caudate nuclei (black arrows), and globus pallidus (white arrows). **(b)** CT scan obtained through the posterior fossa demonstrates that the relatively spared cerebellum has higher attenuation than do the damaged, hypoattenuating supratentorial structures (white cerebellum sign).

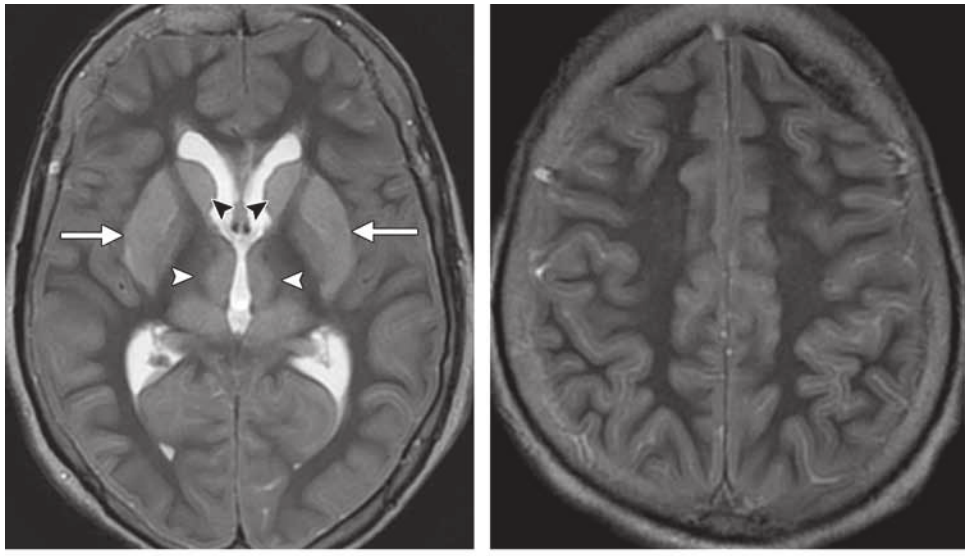

a. b.

Figure 10. HIE in a 38-year-old woman who was resuscitated after being involved in a traffic accident. **(a)** T2-weighted MR image demonstrates bilaterally symmetric hyperintense areas in the thalamus (white arrowheads), basal ganglia, and cerebral cortex. Black arrowheads = caudate nuclei, arrows = lentiform nuclei. **(b)** T2-weighted MR image obtained at a higher level more clearly depicts diffuse cortical involvement.

Hypoxic Ischemic Encephalopathy

HIE of the brain in adults may be the result of circulatory or respiratory failure from causes including cardiac arrest, drowning, or asphyxiation. In most of these cases, the clinical findings are obvious. Neuroimaging findings depend on the severity of the insult, the timing of the study, and the age of the patient, with neonatal asphyxia being a special situation with a characteristic distribution of lesions in the immature brain (25).

In adults, mild HIE may affect only the watershed zones. Severe HIE characteristically affects

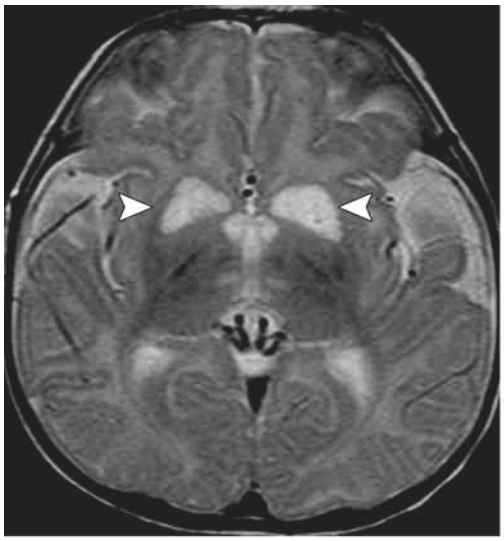

a.

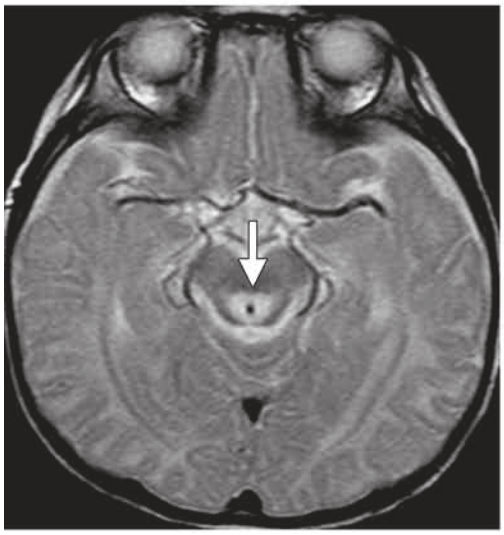

b.

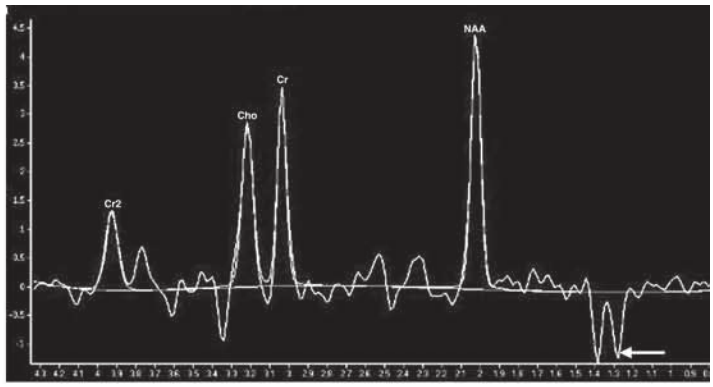

c.

Figure 11. Leigh disease in an 11-month-old boy who presented with irritability and failure to thrive. **(a, b)** Axial T2-weighted MR images obtained at the level of the deep gray nuclei **(a)** and through the posterior fossa **(b)** reveal symmetric areas of hyperintensity in the putamina (arrowheads in **a**) and periaqueductal region (arrow in **b**). **(c)** Spectrum from MR spectroscopy performed with an echo time of 144 msec with the voxel placed over the region of interest reveals an inverted double peak at 1.33 ppm (arrow), a finding that is characteristic of lactate accumulation in Leigh disease. *Cho* = choline, *Cr* = creatine, *NAA* = *N*-acetylaspartate.

the gray matter structures, including the cerebral cortex, basal ganglia, and hippocampi. The thalamus and cerebellum may also be affected, but the brainstem and cerebral white matter are typically spared. CT findings include diffuse edema, decreased attenuation of the cortical gray matter with loss of normal gray matter–white matter differentiation, and bilateral decreased attenuation of the basal ganglia and thalamus (Fig 9a) (26). The "reversal sign" may be seen, in which there is higher attenuation in the white matter, reversing the normal relative attenuation between white matter and gray matter. Diffuse cerebral damage results in a lower attenuation compared with the cerebellum and brainstem, which are relatively spared, resulting in the "white cerebellum sign" (Fig 9b). These findings in severe HIE usually indicate a poor prognosis (27).

The earliest finding at MR imaging (after 2 hours) is increased signal intensity of the affected areas on diffusion-weighted images (27). Conventional T2-weighted images demonstrate subtle increased signal intensity and swelling of the affected areas, usually 24 hours or more after the insult (Fig 10). Delayed postanoxic leukoencephalopathy may result in diffuse T2 prolongation in the subcortical white matter (25).

Leigh Disease

Leigh disease (subacute necrotizing encephalomyelopathy) is a mitochondrial disease that results from a disorder in the respiratory chain production of adenosine triphosphate. Clinical manifestations can be highly variable, affecting children and (rarely) young adults and typically causing central hypotonia, developmental regression or arrest, ophthalmoplegia, respiratory and bulbar dysfunction, and ataxia.

MR imaging findings include symmetric areas of T2 prolongation in the basal ganglia, periaqueductal region, and cerebral peduncles, with putaminal involvement being a consistent feature (Fig 11a, 11b) (28). When Leigh disease is suspected, MR spectroscopy (best performed with long echo times) may reveal the presence of abnormally high lactate levels in the basal ganglia (Fig 11c), which together with elevated serum and CSF lactate levels supports the diagnosis (29).

Wilson Disease

Wilson disease is caused by the accumulation of copper resulting from a deficiency of ceruloplasmin, its serum transport protein. This disease, also known as hepatolenticular degeneration, affects the liver, brain, and other tissues. The symptoms vary and include dysarthria, dystonia, tremors, ataxia, Parkinsonian symptoms, and psychiatric problems. Kayser-Fleisher rings in the cornea are characteristically associated with Wilson disease.

MR imaging findings include areas of T2 prolongation in the putamen (a common finding), globus pallidus, caudate nuclei, and thalamus. Thalamic involvement is typically confined to the ventrolateral aspect (Fig 12) (30). The cortical and subcortical regions, mesencephalon, pons, vermis, and dentate nuclei may also be involved. Diffusion restriction is often seen in the early stages of the disease (31,32).

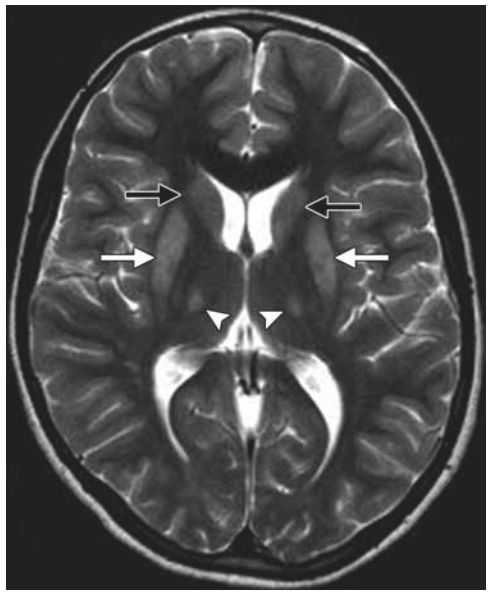

Figure 12. Wilson disease in a 9-year-old boy with tremors and dystonia. T2-weighted MR image depicts bilaterally symmetric areas of abnormal T2 prolongation in the ventrolateral thalamus (arrowheads), putamina (white arrows), and caudate nuclei (black arrows).

Osmotic Myelinolysis

Central pontine myelinolysis and *extrapontine myelinolysis* are terms used to describe a syndrome of demyelination involving the pons and the extrapontine structures, respectively. Osmotic demyelination is associated with electrolyte imbalances (in particular, rapid overcorrection of hyponatremia) and may be seen in chronically alcoholic patients, malnourished patients, or chronically debilitated organ transplant recipients (33,34). The clinical manifestations are variable and include spastic hemiparesis, pseudobulbar palsy, decreased levels of consciousness, and coma.

Oligodendroglial cells are most susceptible to osmotic stresses, and the distribution of changes at MR imaging parallels the distribution of these cells in the central pons, thalamus, putamen, lateral geniculate bodies, and other extrapontine sites (33). Abnormal T2 and T1 prolongation are seen in the affected areas at MR imaging. In central pontine myelinolysis, a symmetric trident-shaped or bat wing–shaped area of increased signal intensity in the central pons is characteristically seen on T2-weighted and fluid-attenuated inversion recovery MR images. The ventrolateral pons and the pontine portion of the corticospinal tracts are typically spared (35).

Extrapontine myelinolysis manifests as areas of T2 prolongation in the globus pallidus, putamen, thalamus, and cerebellum (Fig 13) (34). The lesions may sometimes show restricted diffusion at diffusion-weighted MR imaging in the early stages of the disease process, although this is not typical. Serial measurements of serum sodium levels may be helpful for diagnosis.

Wernicke Encephalopathy

Wernicke encephalopathy typically results from a vitamin B1 (thiamine) deficiency, secondary to a malnourished state caused by (for example) chronic alcoholism, gastrointestinal or hematologic neoplasms, chronic dialysis, bowel obstruction, hyperemesis gravidarum, or prolonged parenteral therapy without vitamin supplementation. The classic clinical triad of altered consciousness, ocular dysfunction, and ataxia is not always present at clinical onset, and the symptoms may be confusing. Wernicke encephalopathy represents a medical emergency, and treatment consists of intravenous replacement of thiamine (36).

Typical findings at MR imaging include symmetric T2 prolongation in the medial thalamus, periaqueductal area, mamillary bodies, and tectal plate (Fig 14) (37). Petechial hemorrhage, diffusion restriction, and contrast enhancement of the affected areas may be noted. Zuccoli et al (37) noted that involvement of the mamillary bodies was most prevalent in chronic alcohol abusers.

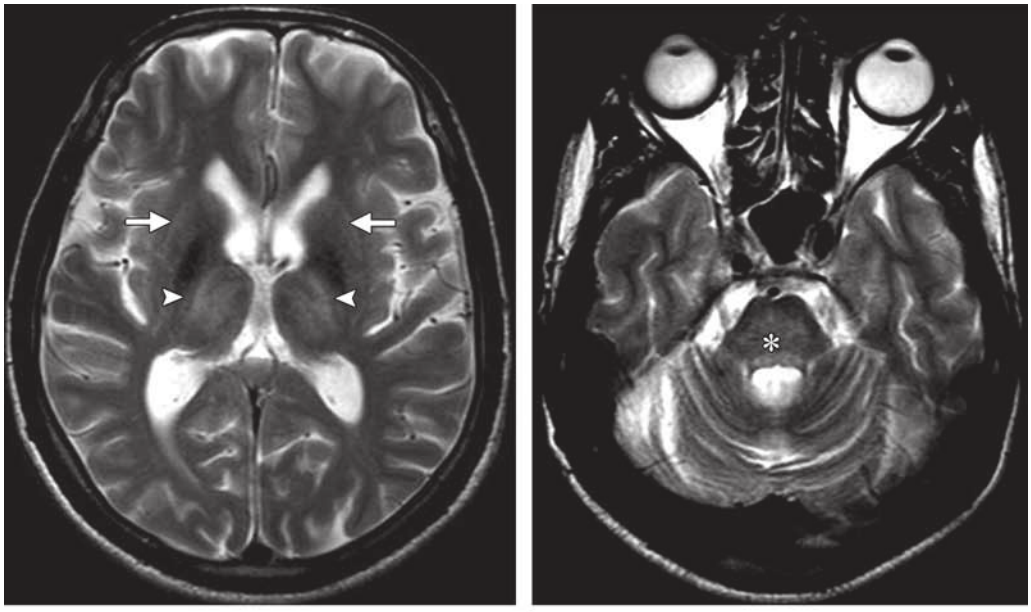

a. b.

Figure 13. Osmotic myelinolysis in a 59-year-old alcoholic man who presented with confusion and pseudobulbar palsy. **(a)** T2-weighted MR image depicts bilaterally symmetric hyperintense areas in the thalamus (arrowheads) and putamina (arrows). **(b)** T2-weighted MR image obtained inferior to **a** demonstrates an ill-defined hyperintense area in the central pons (*), with sparing of the rim.

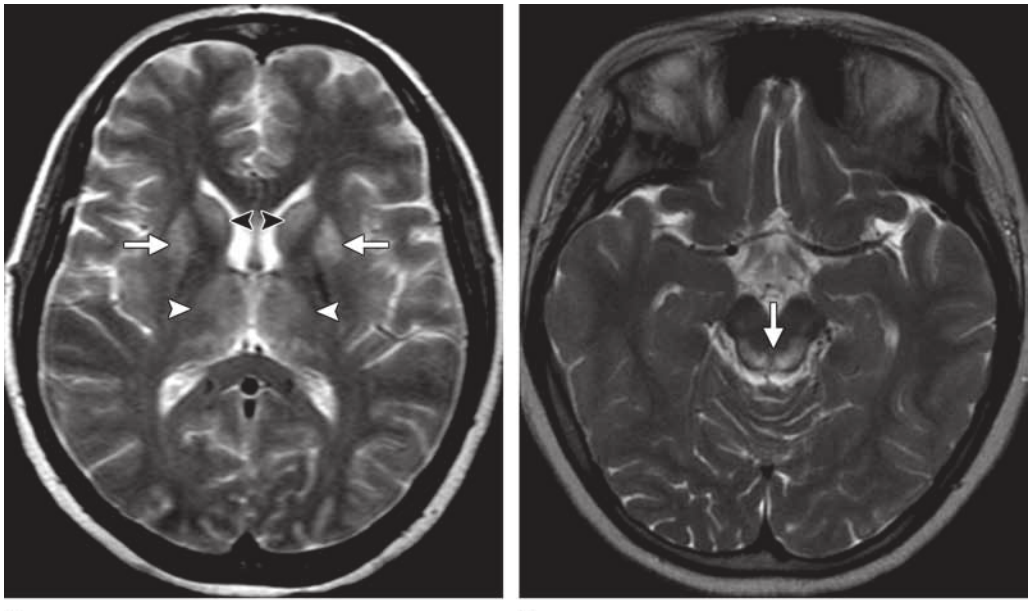

a. b.

Figure 14. Wernicke encephalopathy in a 36-year-old alcoholic man with impaired consciousness. **(a)** Axial T2-weighted MR image shows bilaterally symmetric areas of T2 prolongation in the paramedian thalamus along the third ventricle (white arrowheads), the caudate nuclei (black arrowheads), and the putamina (arrows). **(b)** Axial T2-weighted MR image shows ill-defined hyperintense areas in the periaqueductal region (arrow).

Neurodegeneration with Brain Iron Accumulation

NBIA is a heterogeneous group of disorders characterized by brain degeneration and excessive iron deposition in the basal ganglia. Two clinical categories are recognized: *(a)* classic early-onset, rapidly progressive disease; and *(b)* atypical late-onset, slowly progressive disease (38). In classic NBIA and in one-third of cases of atypical disease, the PANK2 gene is mutated. This gene encodes a pantothenate kinase, and affected patients (with pantothenate kinase–associated neurodegeneration [previously known as Hallervorden-Spatz disease]) typically present with pyramidal or extrapyramidal signs, dystonia, and dysarthria (38,39).

In NBIA, the diagnostic MR imaging feature is bilateral hypointensity in the globus pallidus at T2-weighted imaging, which correlates with iron accumulation observed at pathologic examination. Patients with pantothenate kinase–associated neurodegeneration with the PANK2 mutation demonstrate the "eye-of-the-tiger sign," with a high-signal-intensity center surrounded by the more typical hypointensity in the globus pallidus (Fig 15) (40). The eye-of-the-tiger sign is not seen in PANK2 mutation–negative patients (38).

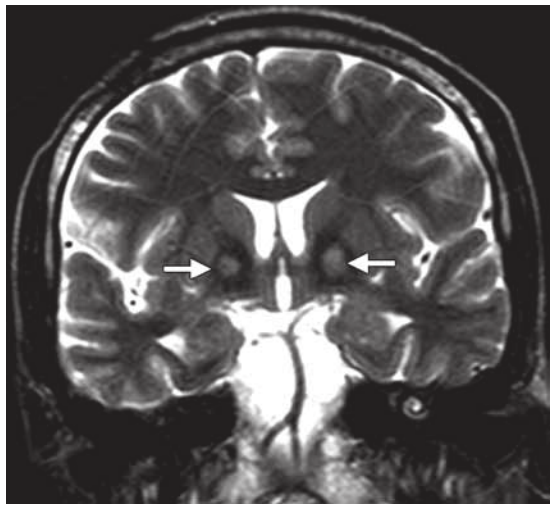

Figure 15. Pantothenate kinase–associated neurodegeneration (Hallervorden-Spatz disease) in a 24-year-old man with dystonia. Coronal T2-weighted MR image demonstrates bilateral hyperintense pallidal areas on background areas of T2 shortening (eye-of-the-tiger sign) (arrows). (Courtesy of Shrinivas Desai, MD, Jaslok Hospital and Research Centre, Mumbai, India.)

Creutzfeldt-Jakob Disease

CJD is a transmissible fatal neurodegenerative disorder caused by prions (self-replicating proteinaceous infectious particles). There are four main subtypes: sporadic, familial, iatrogenic, and variant CJD, with the latter being associated with bovine spongiform encephalopathy ("mad cow disease"), transmitted through consumption of bovine spongiform encephalopathy–contaminated meat. Patients with CJD typically present with rapidly progressive dementia, myoclonus, and multifocal neurologic dysfunction. Brain biopsy or autopsy is required for a definitive diagnosis (41). Diffusion-weighted MR imaging, despite its sensitivity, is currently not part of the criteria for the probable diagnosis of sporadic CJD, and generalized periodic sharp wave complexes at electroencephalography or the detection of 14-3-3 proteins in the CSF are still required for noninvasive diagnosis (42–44).

Nevertheless, diffusion-weighted MR imaging has become increasingly important for the diagnosis of sporadic CJD, with the cerebral cortex and basal ganglia typically being involved (Fig 16). Restricted diffusion seen at diffusion-weighted MR imaging is attributed to spongiform neuronal degeneration and is more sensitive than T2-weighted imaging findings in detecting CJD, especially for cortical lesions (44).

Teaching Point

Variant CJD is associated with bovine spongiform encephalopathy and the typical bilateral lesions in the pulvinar nuclei of the thalamus (pulvinar sign or hockey stick sign) (45). Although thalamic involvement was first described as the key finding in variant CJD, the thalamus may also be involved (typically with other abnormalities) in the more common sporadic form of CJD (46).

Fahr Disease

Fahr disease (also known as bilateral striopallidodentate calcinosis) is a rare neurodegenerative disease that is characterized by the bilaterally symmetric deposition of calcium (and other minerals) in the basal ganglia, thalamus, dentate

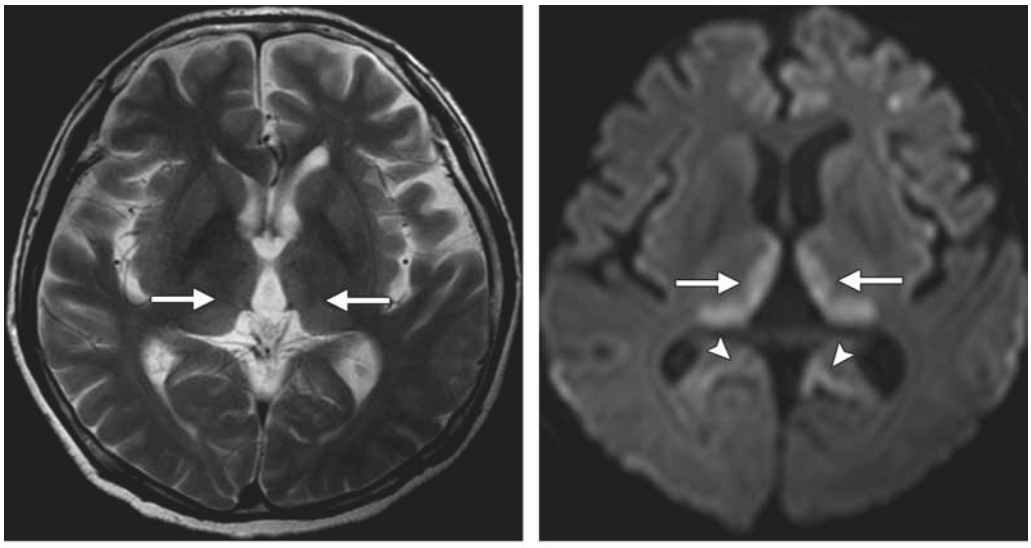

a. b.

Figure 16. CJD in a 71-year-old man with rapidly progressive dementia and myoclonus. T2-weighted **(a)** and diffusion-weighted **(b)** MR images reveal bilaterally symmetric areas of T2 prolongation and restricted diffusion in the medial pulvinar nuclei of the medial thalamus ("pulvinar sign" or "hockey stick sign") (arrows). The affected sites are better seen on the diffusion-weighted MR image. Note the high signal intensity of the cingulate gyri (arrowheads in **b**). Sporadic CJD was confirmed at autopsy.

Figure 17. Fahr disease in a 44-year-old man with dementia and gait disturbances. Noncontrast CT scan shows bilaterally symmetric high-attenuation calcifications in the thalamus, caudate nuclei, putamina, globus pallidus, and subcortical white matter.

nuclei, and centrum semiovale in the absence of hypoparathyroidism. Patients present with a slow onset of nonspecific symptoms such as headache, vertigo, movement disorders, syncope, and seizures. Other neurologic deficits include paresis, spasticity, gait disturbance, speech disorders, coma, dementia, Parkinsonism, chorea, tremors, dystonia, myoclonia, and orthostatic hypotension.

At neuroimaging, the condition is characterized by bilaterally symmetric dense calcifications in the basal ganglia, dentate nuclei, thalamus, and subcortical white matter of the cerebrum (Fig 17). Important alternatives in the radiologic differential diagnosis for Fahr disease include hypoparathyroidism or pseudohypoparathyroidism (end-organ resistance to parathyroid hormone), which can be confirmed with measurements of serum calcium, phosphorus, and parathyroid hormone levels (47,48). Pseudopseudohypoparathyroidism, in which there is no abnormality of calcium metabolism in asymptomatic patients, is another possible diagnosis in patients with widespread cerebral calcification (48).

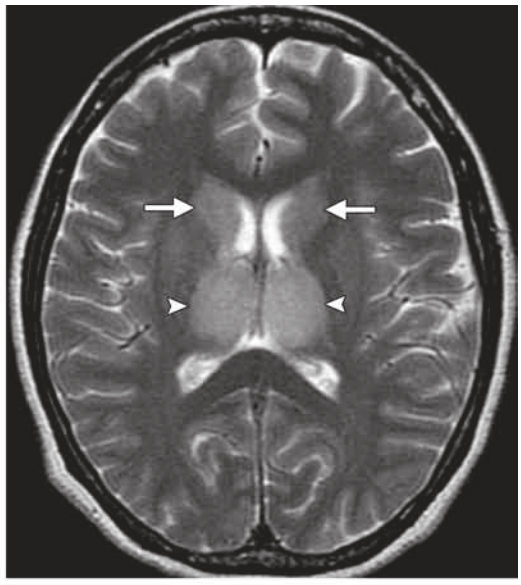

a.

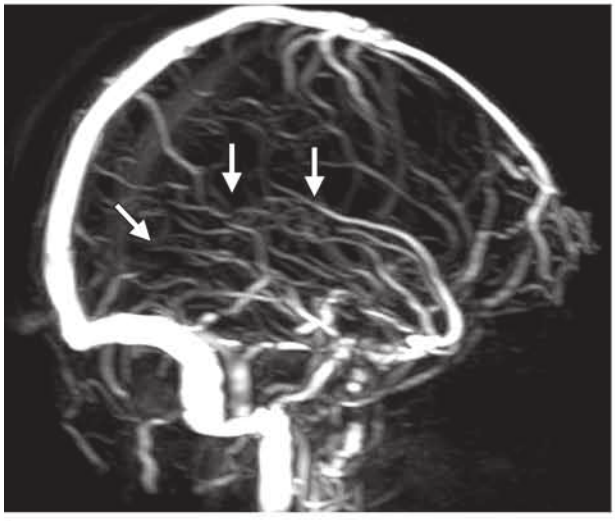

b.

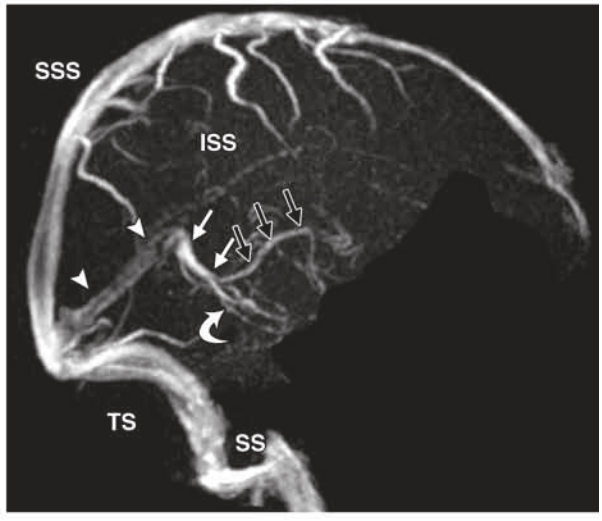

c.

Figure 18. Deep CVT in a 37-year-old woman with headache and drowsiness. **(a)** T2-weighted MR image shows bilateral hyperintense areas in the thalamus (arrowheads) and caudate heads (arrows). **(b)** Phase-contrast MR venogram shows absence of normal flow in the internal cerebral veins, vein of Galen, and straight sinus (arrows), with preservation of the superior sagittal and transverse sinuses. **(c)** Phase-contrast MR venogram obtained in a different patient depicts the internal cerebral veins (black arrows); basal vein of Rosenthal (curved arrow); and vein of Galen (straight white arrows), which drains into the straight sinus (arrowheads). *ISS* = inferior sagittal sinus, *SS* = sigmoid sinus, *SSS* = superior sagittal sinus, *TS* = transverse sinus. (Reprinted, with permission, from reference 50.)

Deep Cerebral Venous Thrombosis

Cerebral venous thrombosis (CVT) is usually associated with risk factors such as a hypercoagulable state during pregnancy or puerperium, use of oral contraceptives, vasculitis, and intracranial or systemic infections (49). Thrombosis of the superficial dural sinus system (the superior and inferior sagittal sinuses, transverse sinuses, and cortical veins) typically results in cerebral edema and venous infarction of the cerebral cortex near the vertex. However, involvement of the deep venous system (the internal cerebral vein, vein of Galen, and straight sinus) can result in a different distribution of venous hypertension. Deep CVT often occurs as an extension of widespread superficial dural sinus CVT; in rare instances, however, it may occur in isolation, with bilateral involvement of the thalamus and basal ganglia without cerebral lobar venous infarction (Fig 18a) (50). Patients present with acute headache, nausea, vomiting, seizures, and altered mental status. Focal neurologic deficits, coma, and death may ensue in severe cases.

At neuroimaging, venous hypertension and cerebral edema caused by deep CVT typically result in T2 prolongation in the thalamus, usually involving the internal capsule, basal ganglia, and deep white matter as well. Hemorrhagic conversion is common, resulting in decreased signal with all pulse sequences, but especially with gra-

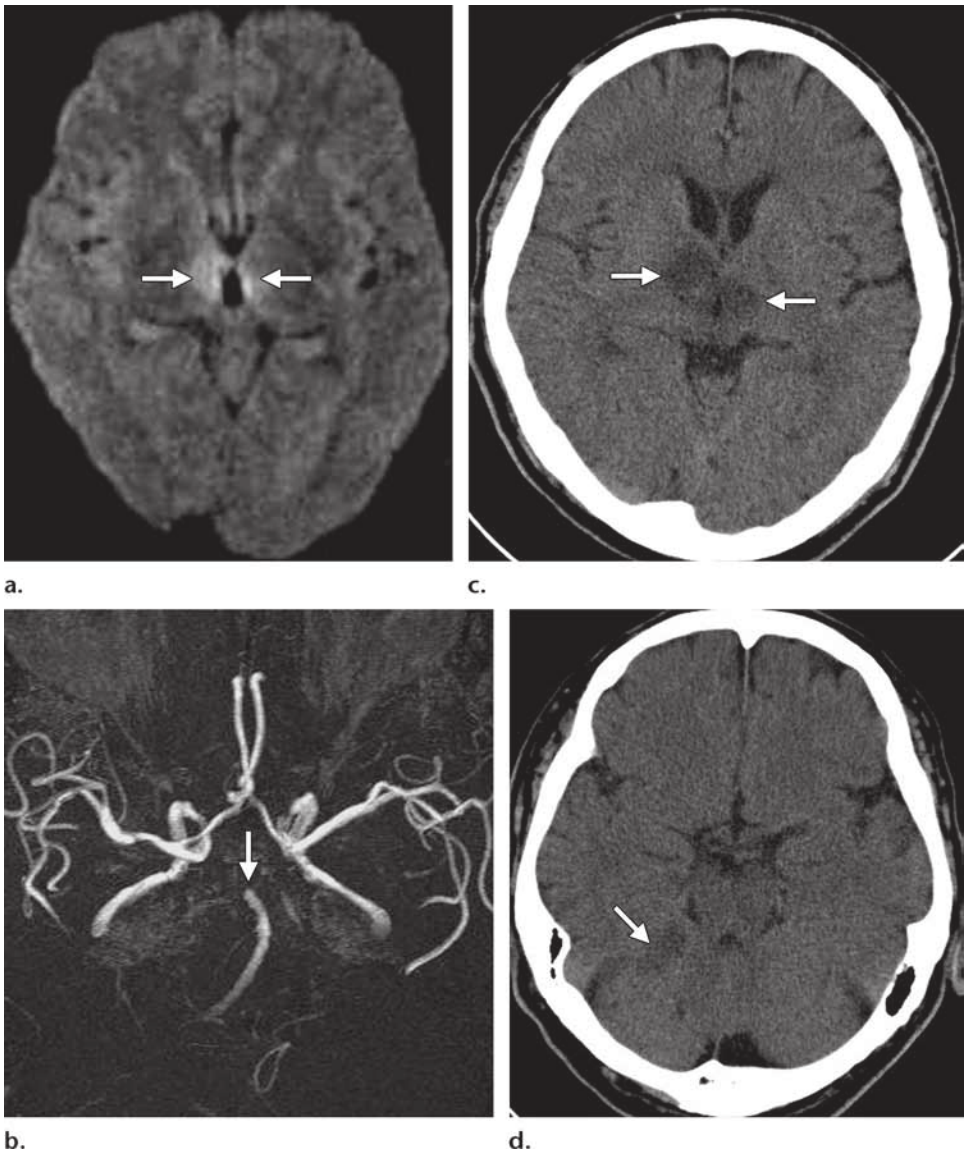

Figure 19. Basilar artery occlusion in a 61-year-old man with ocular signs and severe obtundation. **(a)** Diffusion-weighted MR image shows bilateral hyperintense areas in the paramedian thalamus (arrows). **(b)** Time-of-flight MR angiogram clearly depicts occlusion of the rostral portion of the basilar artery (arrow). **(c, d)** Noncontrast CT scans obtained 3 days later show bilateral subacute infarcts of the thalamus (arrows in **c**) and an infarct in the right cerebellar hemisphere (arrow in **d**).

dient-recalled echo sequences. Diffusion restriction at diffusion-weighted MR imaging has been described in CVT by some authors but is not a consistent feature (51).

Teaching Point

Simultaneous bilateral involvement of the thalamus and basal ganglia in the appropriate clinical setting should prompt a search for subtle signs of venous thrombosis such as loss of flow void and hyperintense thrombus in the straight sinus, vein of Galen, and internal cerebral veins on conventional MR images (52). The addition of MR venography (and, increasingly, CT venography) to the imaging protocol allows the evaluation of thrombosis of the superficial venous sinuses, which is often diagnostic for deep CVT (Fig 18b, 18c).

Arterial Occlusion

Bilateral acute synchronous arterial infarctions of the thalamus are not uncommon, and are usually the result of occlusion of the rostral basilar artery. Patients with thalamic infarction typically present with agitation, obtundation or coma, memory dysfunctions, and various types of ocular and behavioral changes.

These acute infarcts characteristically demonstrate hyperintensity on T2-weighted MR images and restricted diffusion on diffusion-weighted images (Fig 19a), and the causative steno-occlusive disease involving the basilar artery is often well depicted on MR angiograms (Fig 19b) (53,54).

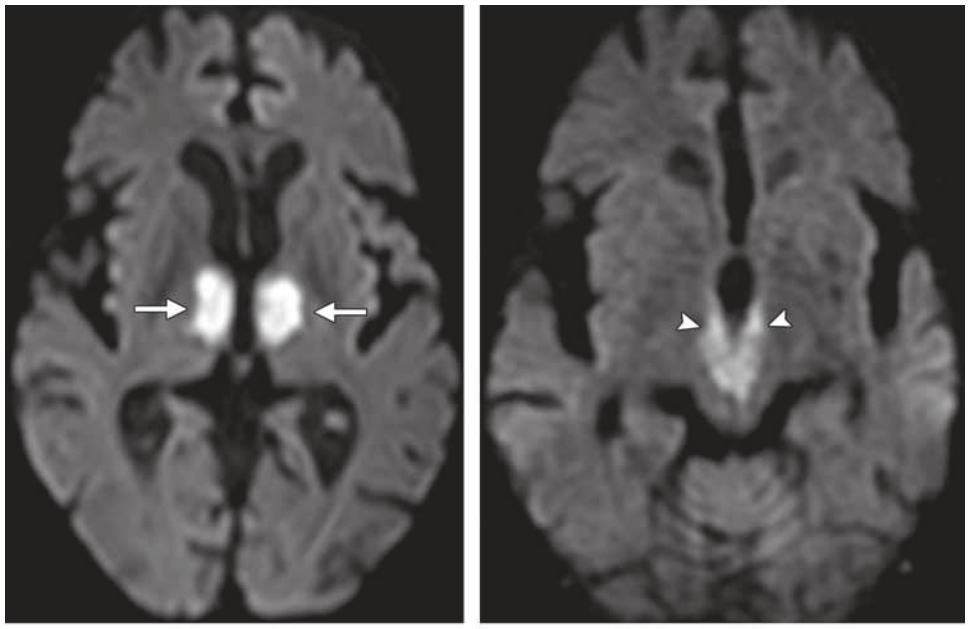

a. b.

Figure 20. Occlusion of the artery of Percheron in a comatose 67-year-old man. Diffusion-weighted MR images show hyperintense areas in the paramedian thalamus (arrows in **a**) and midbrain (arrowheads in **b**).

In addition to affecting the thalamus, thrombosis of the rostral basilar artery typically also causes acute infarction of the midbrain and portions of the temporal and occipital lobes fed by the posterior cerebral artery, or of portions of the cerebellum fed by other branches of the vertebrobasilar arterial system (Fig 19c, 19d).

A rare cause of bilaterally symmetric thalamic infarction is occlusion of the artery of Percheron, an anatomic variant of the posterior circulation. The blood supply of the normal thalamus and midbrain may show several variants (55,56). In one of the three arterial variants described by Percheron, a common trunk (the artery of Percheron) arises from the first segments of the posterior cerebral artery on one side but supplies the thalamus and midbrain on both sides. Occlusion of this common trunk results in bilaterally symmetric infarctions in the paramedian portions of the thalamus and brainstem (Fig 20) (57). Although cerebral infarction has a distinctive anatomic distribution in Percheron arterial occlusion, the depiction of the artery of Percheron itself at MR angiography or digital subtraction angiography has not been well described in the literature (57).

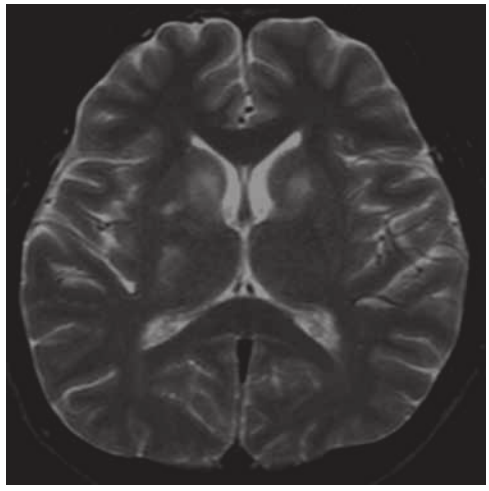

Figure 21. Neuro-Behçet disease in a 49-year-old man with headache and personality disorders. Axial T2-weighted MR image reveals poorly defined areas of T2 prolongation in both caudate nuclei and the right lentiform nucleus.

Neuro-Behçet Disease

Behçet disease is a multisystemic, recurrent inflammatory disorder of unknown cause; autoimmune, infectious, and genetic causes have all

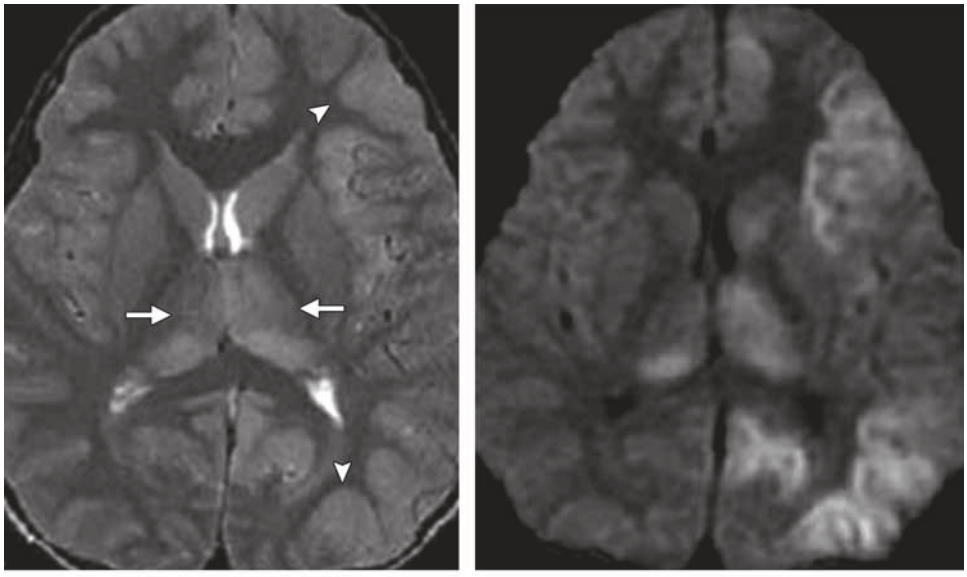

a. b.

Figure 22. Seropositive Japanese B encephalitis in a 14-year-old boy with fever and malaise. T2-weighted **(a)** and diffusion-weighted **(b)** MR images reveal asymmetric ill-defined hyperintense areas in the thalamus (arrows in **a**) and the left frontal and parieto-occipital cortex (arrowheads in **a**).

been postulated as responsible for the classic clinical triad of uveitis, oral ulcers, and genital ulcers (58). The CNS is affected in 4%–49% of patients with Behçet disease, which has a predilection for men and has a higher prevalence in the eastern Mediterranean, the Middle East, and Japan. Although ulcerative symptoms of Behçet disease usually precede neurologic complications (eg, headache, dysarthria, cerebellar signs, sensory signs, personality change), 3% of cases manifest initially in the CNS. In these cases, radiologic diagnosis becomes a challenge, especially since there are no confirmatory chemical or serologic investigations (59).

Focal or multifocal lesions are common in neuro-Behçet disease, with rarer forms manifesting with meningoencephalitis and CVT (58). The sites most commonly involved by focal lesions include the brainstem, basal ganglia (bilateral involvement in one-third of cases), and thalamus (Fig 21) (59), and, less commonly, the white matter of the cerebral hemispheres and cervicothoracic spinal cord. These lesions are hyperintense on T2-weighted MR images, are hypointense on T1-weighted images, enhance after contrast material administration, and are typically associated with vasogenic edema (60). They are isointense or slightly hyperintense on diffusion-weighted images.

Flavivirus Encephalitis

Flavivirus infections such as Japanese encephalitis, West Nile fever, and Murray Valley fever typically demonstrate symmetric involvement of the deep gray matter structures. The exact reason for this phenomenon is unknown, although the inherent metabolic activity and vascular supply of these structures may play a role (61,62).

The geographic distributions of these viral infections are characteristic but may overlap, with Japanese encephalitis being common in Asia, West Nile fever in the Middle East (now also in North America), and Murray Valley fever in Australia. The clinical presentation typically involves a prodromal phase of fever, rigors, headache, rashes, and body aches followed by CNS symptoms that include dyskinesia, dystonia, tremors, drooling, dysarthria, altered consciousness, seizures, and coma. The definitive serologic diagnosis is based on the detection of antibodies in serum and CSF at enzyme-linked immunosorbent assay.

The most characteristic MR imaging finding of Japanese encephalitis is T2 hyperintensity, typically with bilateral involvement of the posteromedial thalamus (Fig 22a). Intralesional

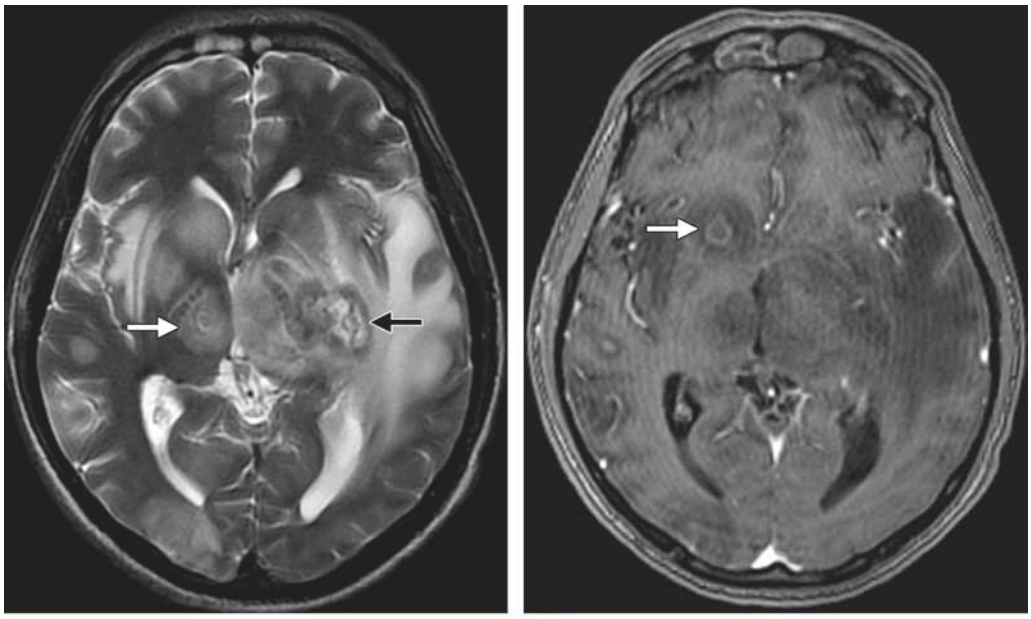

a. b.

Figure 23. CNS toxoplasmosis in a 37-year-old HIV-seropositive man who presented with headache and drowsiness. **(a)** Axial T2-weighted MR image shows multiple bilateral hypointense lesions in the caudate nuclei, left lentiform nucleus (black arrow), and right thalamus (white arrow), with extensive perifocal edema. **(b)** On an axial contrast-enhanced T1-weighted MR image obtained at a lower level, the lesion in the right caudate nucleus demonstrates rim enhancement (arrow).

hemorrhages and restricted diffusion have also been described (Fig 22b) (63,64). Other sites of involvement include the basal ganglia, substantia nigra, red nucleus, pons, hippocampi, cerebral cortex, and cerebellum. Japanese encephalitis and Murray Valley encephalitis more often involve the thalamus (62), whereas West Nile fever typically demonstrates bilateral involvement of the thalamus and the caudate and lentiform nuclei (61).

Cerebral Toxoplasmosis

Cerebral toxoplasmosis is an opportunistic infection caused by the protozoan *Toxoplasma gondii*, typically in immunocompromised patients such as those with human immunodeficiency virus (HIV) infection and acquired immunodeficiency syndrome (AIDS). CNS involvement leads to fever, headache, and confusion, progressing to coma, focal neurologic deficits, and seizures. Polymerase chain reaction testing of blood samples has been helpful for diagnosis in some studies (65).

At neuroimaging, cerebral toxoplasmosis manifests as multiple focal lesions in the basal ganglia and lobar gray matter–white matter junctions (66,67). On T2-weighted MR images, the lesions are typically hypo- to isointense, usually with prominent associated mass effect and vasogenic edema (Fig 23a). Hemorrhagic lesions may appear hyperintense on T1-weighted images and are hypointense on gradient-recalled echo images. After contrast material injection, nodular or ring enhancement is typically seen (Fig 23b). The conventional MR imaging appearance of basal ganglia toxoplasmosis in patients with HIV-AIDS may be similar to that of CNS lymphoma (discussed in the following section). Thallium-201 single photon emission computed tomography, positron emission tomography, or MR spectroscopy (which typically demonstrates lipid breakdown products without elevated choline levels in toxoplasmosis) may be useful in narrowing the differential diagnosis.

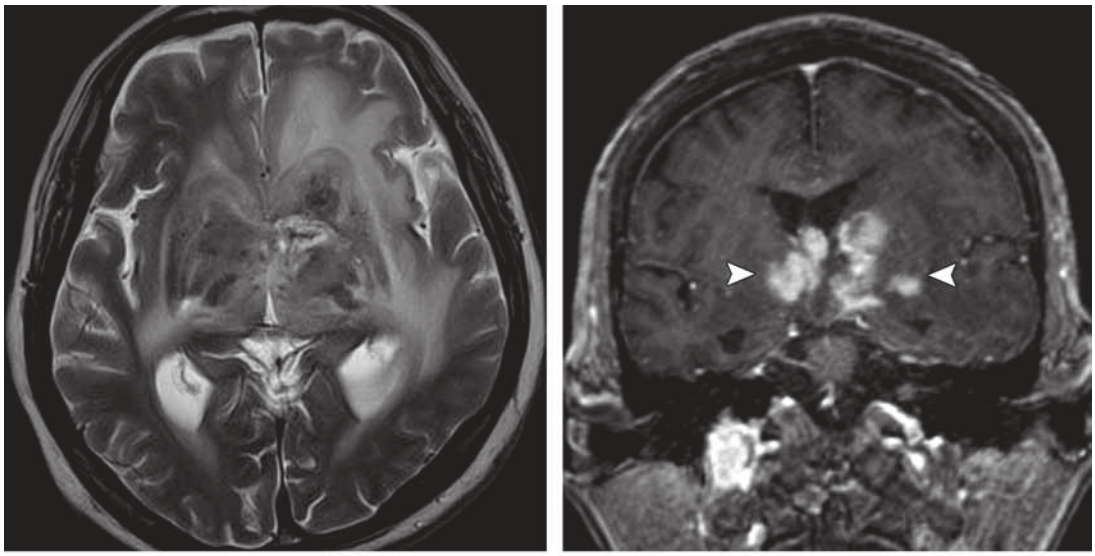

a. b.

Figure 24. Primary CNS lymphoma (confirmed histologically) in a 55-year-old man with headache, altered mental status, and AIDS. **(a)** Axial T2-weighted MR image depicts bilateral ill-defined isointense to hypointense areas involving the basal ganglia and thalamus, with extensive perifocal edema. **(b)** On a coronal contrast-enhanced T1-weighted MR image, the lesions (arrowheads) demonstrate avid enhancement.

Primary CNS Lymphoma

Primary lymphomatous disease of the CNS may be encountered in both immunocompetent and immunocompromised (typically HIV-AIDS) patients. Congenital causes of immunodeficiency and an immunosuppressive treatment regimen after organ transplantation are also associated with a greater risk for primary CNS lymphoma.

Primary CNS lymphoma commonly involves the deep hemispheric periventricular white matter, corpus callosum, and basal ganglia (Fig 24a) (68). Multiple lesions and involvement of the basal ganglia are more common in patients with HIV-AIDS, and lesions may mimic the more common opportunistic infection of toxoplasmosis (discussed earlier). The periventricular location and subependymal spread of primary CNS lymphoma may help distinguish it from CNS toxoplasmosis (67). Advanced imaging methods such as MR spectroscopy (with elevated choline levels) may also be useful in this regard (69). The high attenuation of primary CNS lymphoma at CT and its iso- or hypointensity relative to gray matter at T2-weighted MR imaging have been attributed to high tumor cellularity. Solid, homogeneously enhancing lesions are typical in immunocompetent patients, whereas lesions with ring enhancement and central necrosis occur predominantly in AIDS patients (Fig 24b) (68).

Primary Bilateral Thalamic Glioma

The thalamus is affected in 1%–1.5% of brain tumors, including secondary involvement by contiguous spread of adjacent lesions such as pineal germ cell tumors. PBTG is a rare but characteristic neoplasm that demonstrates bilateral involvement of the thalamus in children and young adults (70). Patients typically present with behavioral impairment ranging from personality changes to dementia. Although PBTG is a low-grade astrocytoma (World Health Organization grade II), patients with PBTG, because of its deep location, have a very poor prognosis despite therapy.

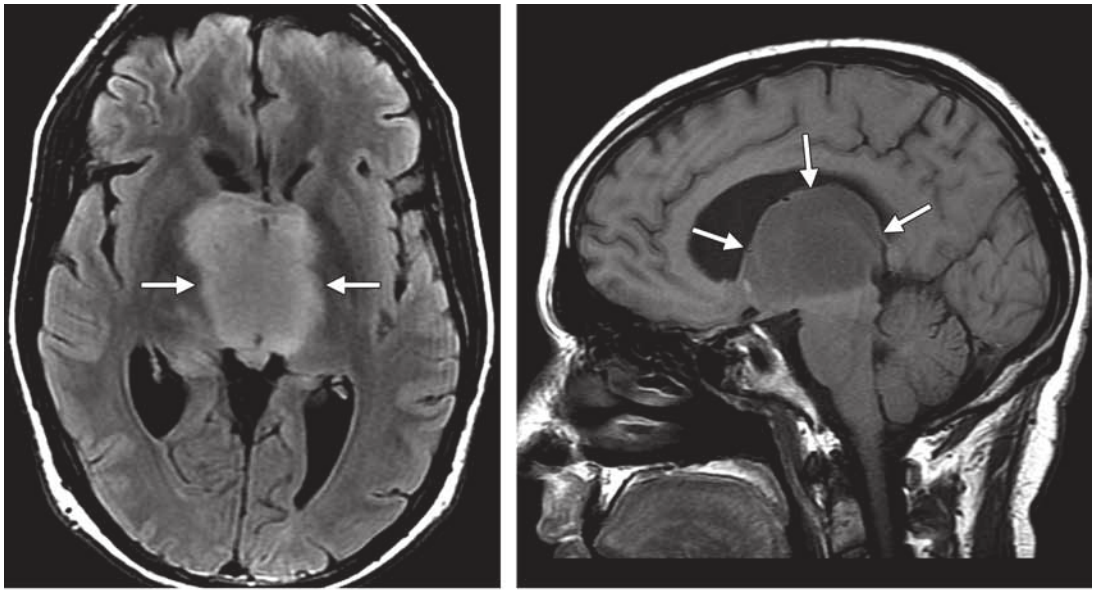

a. b.

Figure 25. PBTG in a 24-year-old man with altered mental status and behavioral changes. **(a)** Axial fluid-attenuated inversion recovery image shows bilaterally symmetric, well-defined hyperintense areas and enlargement of the thalamus (arrows). **(b)** On a sagittal contrast-enhanced T1-weighted MR image, the thalamus (arrows) demonstrates diffuse hypointensity.

CT and MR imaging typically reveal a mass that symmetrically enlarges both sides of the thalamus (70–72). At MR imaging, PBTG appears hyperintense on T2-weighted images and isointense on T1-weighted images. Typically, these tumors do not enhance on postcontrast T1-weighted images (Fig 25). Low-grade PBTGs are characterized by the absence of tumor progression on serial MR images, with tumors remaining within the thalamus respecting the border between gray matter and white matter (72).

Neurofibromatosis Type 1

Neurofibromatosis is the most common phakomatosis (neurocutaneous syndrome) and can be transmitted as an autosomal dominant trait or arise from spontaneous mutations. Clinically, neurofibromatosis type 1 is diagnosed on the basis of the presence of café-au-lait spots, axillary freckling, Lisch nodules, neurofibromas, plexiform neurofibromas, optic glioma, bone dysplasias, or pseudoarthrosis.

MR imaging of the brain may reveal focal areas of increased signal intensity on T2-weighted images, often with T1 shortening (Fig 26). Some studies have reported that the globus pallidus is the most common site of involvement, often on both sides, but these bright objects can also be found in the brainstem and cerebellum (73). They typically exert no mass effect, are not associated with surrounding edema, and do not enhance after contrast material injection. The histologic correlate of these bright objects is not well established, and they may represent hamartomas or vacuolar or spongiotic change (74). These lesions are usually asymptomatic in neurofibromatosis type 1 and may be differentiated from gliomas at MR spectroscopy due to their higher *N*-acetylaspartate–choline, *N*-acetylaspartate–creatine, and creatine-choline ratios (75).

Radiologic Assessment of Abnormalities of the Basal Ganglia and Thalamus

The radiologist may diagnose abnormalities of the basal ganglia or thalamus in patients in different clinical situations. Often, there are typical

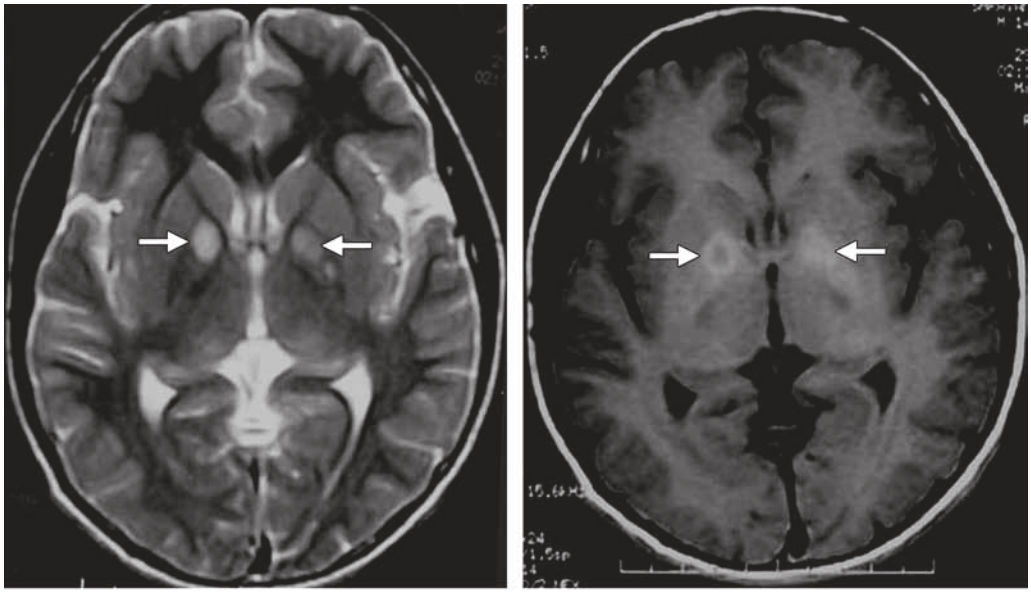

a. b.

Figure 26. "Bright objects" in an asymptomatic 21-year-old woman with neurofibromatosis type 1. **(a)** Axial T2-weighted MR image shows bilateral pallidal areas of hyperintensity (arrows) that have no mass effect. **(b)** On an axial T1-weighted MR image, the foci (arrows) appear hyperintense.

scenarios, signs, or symptoms that lead to neuroimaging examination, such as a known suicide attempt, cardiac arrest, diabetic hypoglycemia, hyperglycemic chorea-ballismus, or HIV-AIDS, or risk for vitamin deficiency and electrolyte imbalance. In such cases, imaging abnormalities of the deep gray matter nuclei usually confirm the clinical suspicion. Sometimes, however, the clinical diagnosis is not apparent, there are few positive signs, or the clinical presentation is nonspecific or misleading. In some of these situations, the radiologist may detect an unsuspected but readily apparent abnormality at CT or MR imaging, and the characteristic pattern at neuroimaging may be the first indicator of the correct diagnosis (14). Although often typical, the clinical and neuroimaging findings may overlap or change during acute exacerbations of systemic disease, such as exacerbations in Leigh disease, delayed leukoencephalopathy in carbon monoxide poisoning, or acute hyperammonemic brain damage in decompensated chronic cirrhosis (Fig 6).

Once bilateral lesions of the basal ganglia or thalamus are detected by the radiologist, the appropriate confirmatory clinical and laboratory investigations may be suggested to confirm the diagnosis. These may include serologic studies or immunoassays for toxoplasmosis and flaviviruses; electroencephalography and CSF investigations for CJD; vitamin B1 assays for Wernicke encephalopathy; and determination of *(a)* serum sugar levels for hypoglycemia and hyperglycemia; *(b)* serum sodium levels and osmolarity for osmotic myelinolysis; *(c)* serum ceruloplasmin levels for Wilson disease; *(d)* lactate levels in the serum and CSF for Leigh disease; and *(e)* serum calcium, phosphorus, and parathyroid hormone levels for Fahr disease–hypoparathyroidism and its variants.

Teaching Point

Bilaterally symmetric diffuse abnormalities involving the lentiform and caudate nuclei in their entirety typically suggest systemic or metabolic causes, whereas asymmetric, focal, or discrete lesions affecting only part of the basal ganglia tend to indicate involvement by infections or neoplasms. However, there is often overlap, and atypical features of systemic disease such as unilateral involvement may sometimes cause confusion (21). The thalamus is usually involved together with the basal ganglia in a wide range of conditions such

as hypoxia, osmotic myelinolysis, Wilson disease, Leigh disease, Fahr disease, CJD, deep CVT, infections, and primary CNS lymphoma. Involvement of the basal ganglia but not the thalamus is characteristically caused by systemic disease (toxic poisoning, hypoglycemia, hyperglycemia, liver disease, Huntington disease, NBIA, neurofibromatosis), whereas bilateral thalamic involvement with no abnormality of the basal ganglia is less common and more often due to focal (arterial occlusion, flavivirus infection, PBTG), rather than generalized (Wernicke encephalopathy), abnormalities.

The detection of associated abnormalities in parts of the brain other than the basal ganglia and thalamus is also helpful in narrowing the differential diagnosis. These findings include diffuse or focal cortical involvement in hypoxia, hypoglycemia, and CJD, and diffuse or bilateral white matter abnormalities in poisoning and hypoglycemia. The brainstem may be involved in Leigh disease, osmotic myelinolysis, neuro-Behçet disease, and basilar artery occlusion. Basilar artery occlusions typically also affect the arterial territory supplied by the posterior cerebral artery and other branches of the posterior circulation (both sides of the thalamus, midbrain, occipital and temporal lobe cortex, cerebellum). On the other hand, simultaneous lesions of the thalamus and basal ganglia are consistent with venous but not arterial infarction. These deep nuclear structures are drained by the same deep internal cerebral veins but are supplied by the posterior and anterior arterial circulations, respectively. Therefore, widespread basilar or posterior cerebral artery occlusion typically involves the thalamus as well as the occipital-temporal cortex, not the thalamus and the basal ganglia. MR or CT arteriography and venography would also be helpful in making the correct diagnosis, as would diffusion-weighted MR imaging (discussed in the following paragraph). Finally, CNS infections and tumors may show perilesional edema or infiltration outside the basal ganglia and thalamus, or multifocal disease elsewhere in the brain and meninges.

T2-weighted MR imaging is highly informative in the study of abnormalities of the deep gray matter nuclei, with most acute diseases demonstrating increased signal intensity. Very often, T1-weighted MR imaging and CT also have an important role to play, especially if abnormalities of hyperintensity (in hepatic disease and manganese deposition, hyperglycemia, or neurofibromatosis type 1) may help narrow the differential diagnosis. The presence of calcium (Fahr disease, hypoparathyroidism) and hemorrhage (poisoning, CNS toxoplasmosis, venous infarction, Japanese encephalitis) may also be helpful. The contributions of diffusion-weighted MR imaging in the detection of acute cytotoxic brain damage in acute infarction, hypoxia, hypoglycemia, CJD, and Wernicke encephalopathy have been well described. MR spectroscopy may have a role in detecting lactate in hypoxia or mitochondrial disease and in differentiating opportunistic infection from neoplasm in AIDS. These modalities may be added to the radiologist's toolkit to improve the confidence and timeliness of diagnosis.

Conclusions

Systemic and metabolic abnormalities often involve the basal ganglia or thalamus on both sides, and careful assessment of brain abnormalities occurring simultaneously outside these structures is important. CT and MR imaging, including T1-weighted imaging, diffusion-weighted imaging, MR angiography, MR venography, and MR spectroscopy, are often helpful in narrowing the differential diagnosis. Oftentimes, however, the diagnosis is not straightforward, and the correlation of typical imaging features with clinical and laboratory data can help make the correct diagnosis (Table).

Clinical and Neuroimaging Features of Causes of Bilateral Abnormalities of the Basal Ganglia and Thalamus

Cause	Salient Imaging Features: Primary Nuclei Affected	Salient Imaging Features: Other Areas of Involvement	Clinical History and Laboratory Features
Toxic Poisoning			
Carbon monoxide	GP (decreased ADC, late T1 shortening)	Delayed leukoencephalopathy	Suicide attempt, elevated serum level of carboxyhemoglobin
Methanol	Putamen (hemorrhagic)	WM edema	Accidental ingestion, optic neuritis, toxicity
Cyanide	Putamen (hemorrhagic)	. . .	Industrial accident, toxicity
Metabolic Diseases			
Liver disease	GP (T1 shortening)	Substantia nigra	Cirrhotic patients with spontaneous portosystemic shunts or a history of TIPS placement
Hyperammonemia	BG (decreased ADC)	Insular cortex, cingulate gyrus	Patients with acute exacerbation of hepatic encephalopathy, inborn errors of metabolism, elevated serum ammonia levels, or urea cycle metabolites in the serum or urine
Nonketotic hyperglycemia	Caudate nucleus and GP (T1 shortening, hyperattenuating at CT)	. . .	Diabetic patients with chorea, ballismus, or an elevated blood sugar level
Hypoglycemia	BG (decreased ADC)	Cortical involvement: hippocampus or diffuse pattern of involvement; WM involvement: commonly in the internal capsule, splenium of the corpus callosum, and so on	Diabetic patients with a therapeutic overdose, elevated blood sugar level, or toxicity*
Hypoxic ischemic encephalopathy	BG and thalamus (decreased ADC)	Cortical involvement: watershed infarcts or diffuse involvement; delayed leukoencephalopathy	Cardiac arrest, asphyxia, near drowning
Leigh disease	BG and thalamus (lactate at MR spectroscopy)	Periaqueductal region, cerebral peduncles	Elevated serum or CSF lactate levels, muscle biopsy for mitochondrial abnormalities, genetic analysis for specific mutations
Wilson disease	BG and ventrolateral thalamus (decreased ADC)	. . .	Kayser-Fleischer rings, low serum level of ceruloplasmin, hepatic abnormalities
Osmotic myelinolysis	BG and thalamus (variable ADC)	Pons: "trident sign" or "bat wing sign"	Alcoholic or malnourished patients, rapid overcorrection of hyponatremia
Wernicke encephalopathy	Thalamus (decreased ADC)	Periaqueductal region, mamillary bodies, tectal plate	Alcoholic or malnourished patients, low serum level of thiamine
Vascular Diseases			
Deep cerebral vein thrombosis	BG and thalamus (hemorrhagic, variable ADC)	Adjacent WM†	Dehydration, puerperium, oral contraceptive usage, infection
Arterial occlusion	Thalamus (decreased ADC)	Posterior cerebral artery territory: midbrain, occipital or temporal cortex‡	Sudden onset of localizing neurologic signs of stroke

(continued)

Clinical and Neuroimaging Features of Causes of Bilateral Abnormalities of the Basal Ganglia and Thalamus *(continued)*

Cause	Salient Imaging Features		Clinical History and Laboratory Features
	Primary Nuclei Affected	Other Areas of Involvement	
Degenerative Diseases			
NBIA	GP ("eye of the tiger" sign [hyperintense center with hypointense rim])	. . .	Genetic analysis for PANK2 mutations
CJD	BG and thalamus (decreased ADC, "pulvinar sign" typical of variant CJD)	Cortex	Rapidly progressive dementia, myoclonus, CSF 14-3-3 protein, generalized periodic sharp wave complexes at electroencephalography, brain biopsy for definitive diagnosis
Fahr disease	BG and thalamus (heavy calcification at CT)	Dentate nuclei, subcortical WM	Normal serum calcium and parathyroid hormone levels exclude hypoparathyroidism and pseudohypoparathyroidism
Inflammatory and Infectious Diseases			
Neuro-Behçet disease	BG and thalamus	Brainstem, WM, spinal cord	Affected patients with uveitis or orogenital ulcers; patients in the eastern Mediterranean region, Middle East, or Japan
Flavivirus encephalitis	BG and thalamus (hemorrhagic)	Cortex, substantia nigra, red nucleus, pons, cerebellum	Patients in Asia (Japanese encephalitis), Australia (Murray Valley fever), or the Middle East or United States (West Nile fever); detection of antibodies at enzyme-linked immunosorbent assay of the serum or CSF
CNS toxoplasmosis	BG and thalamus (hemorrhagic, T2 shortening, lipid or lactate at MR spectroscopy)	Adjacent WM	Immunocompromised patients, findings of *T gondii* at serologic analysis
Neoplasms			
Primary CNS lymphoma	BG and thalamus (slightly hyperattenuating at CT, choline at MR spectroscopy, increased uptake at PET and SPECT	Adjacent and periventricular WM, subependymal spread	Immunocompromised patients
PBTG	Thalamus	. . .	Children and young adults
Neurofibromatosis type 1	GP (T1 shortening)	Cranial neurofibroma, optic glioma, or moya-moya disease	Café-au-lait spots, plexiform neurofibromas, or bone dysplasia

Note.—ADC = apparent diffusion coefficient, BG = basal ganglia, GP = globus pallidus, NF-1 = neurofibromatosis type 1, PET = positron emission tomography, SPECT = single photon emission computed tomography, TIPS = transjugular intrahepatic portosystemic shunt, WM = white matter.
*On rare occasions, abdominal CT is performed to evaluate for insulinoma. †MR venography is recommended. ‡MR angiography is useful.

References

1. Kretschmann HJ, Weinrich W. Neurofunctional systems. In: Kretschmann HJ, Weinrich W, eds. Cranial neuroimaging and clinical neuroanatomy: atlas of MR imaging and computed tomography. 3rd ed. New York, NY: Thieme, 2003; 383–387.
2. Heier LA, Bauer CJ, Schwartz L, Zimmerman RD, Morgello S, Deck MD. Large Virchow-Robin spaces: MR-clinical correlation. AJNR Am J Neuroradiol 1989;10(5):929–936.
3. Bennett JC, Maffly RH, Steinbach HL. The significance of bilateral basal ganglia calcification. Radiology 1959;72(3):368–378.
4. Milton WJ, Atlas SW, Lexa FJ, Mozley PD, Gur RE. Deep gray matter hypointensity patterns with aging in healthy adults: MR imaging at 1.5 T. Radiology 1991;181(3):715–719.
5. Finelli PF, DiMario FJ Jr. Diagnostic approach in patients with symmetric imaging lesions of the deep gray nuclei. Neurologist 2003;9(5):250–261.
6. Schmahmann JD. Vascular syndromes of the thalamus. Stroke 2003;34(9):2264–2278.
7. Osborn A. Diagnostic neuroradiology. St Louis, Mo: Mosby, 1994; 341–363.
8. Kretschmann HJ, Weinrich W. Topography of the neurocranium and its intracranial spaces and structures in multiplanar parallel slices. In: Kretschmann HJ, Weinrich W, eds. Cranial neuroimaging and clinical neuroanatomy: magnetic resonance imaging and computed tomography. 2nd ed. New York, NY: Thieme, 1992; 173–253.
9. Rachinger J, Fellner FA, Stieglbauer K, Trenkler J. MR changes after acute cyanide intoxication. AJNR Am J Neuroradiol 2002;23(8):1398–1401.
10. Ghio AJ, Stonehuerner JG, Dailey LA, et al. Carbon monoxide reversibly alters iron homeostasis and respiratory epithelial cell function. Am J Respir Cell Mol Biol 2008;38 (6):715–723.
11. O'Donnell P, Buxton PJ, Pitkin A, Jarvis LJ. The magnetic resonance imaging appearances of the brain in acute carbon monoxide poisoning. Clin Radiol 2000;55(4): 273–280.
12. Pujol A, Pujol J, Graus F, et al. Hyperintense globus pallidus on T1-weighted MRI in cirrhotic patients is associated with severity of liver failure. Neurology 1993;43(1):65–69.
13. Naegele T, Grodd W, Viebahn R, et al. MR imaging and (1) H spectroscopy of brain metabolites in hepatic encephalopathy: time-course of renormalization after liver transplantation. Radiology 2000;216 (3):683–691.
14. Wong YC, Au WL, Xu MS, Ye J, Lim CC. Magnetic resonance spectroscopy in adult-onset citrullinemia: elevated glutamine levels in comatose patients. Arch Neurol 2007; 64(7):1034–1037.
15. Takanashi J, Barkovich AJ, Cheng SF, Kostiner D, Baker JC, Packman S. Brain MR imaging in acute hyperammonemic encephalopathy arising from late-onset ornithine transcarbamylase deficiency. AJNR Am J Neuroradiol 2003;24(3):390–393.
16. Takanashi J, Barkovich AJ, Cheng SF, et al. Brain MR imaging in neonatal hyperammonemic encephalopathy resulting from proximal urea cycle disorders. AJNR Am J Neuroradiol 2003;24(6): 1184–1187.
17. Lai PH, Tien RD, Chang MH, et al. Chorea-ballismus with nonketotic hyperglycemia in primary diabetes mellitus. AJNR Am J Neuroradiol 1996; 17(6):1057–1064.
18. Lee EJ, Choi JY, Lee SH, Song SY, Lee YS. Hemichorea-hemiballism in primary diabetic patients: MR correlation. J Comput Assist Tomogr 2002;26 (6):905–911.
19. Malouf R, Brust JC. Hypoglycemia: causes, neurological manifestations, and outcome. Ann Neurol 1985;17(5): 421–430.
20. Kao SL, Chan CL, Tan B, et al. An unusual outbreak of hypoglycemia. N Engl J Med 2009;360(7): 734–736.
21. Lim CC, Gan R, Chan CL, et al. Severe hypoglycemia associated with an illegal sexual enhancement product adulterated with glibenclamide: MR imaging findings. Radiology 2009;250(1):193–201.
22. Fujioka M, Okuchi K, Hiramatsu KI, Sakaki T, Sakaguchi S, Ishii Y. Specific changes in human brain after hypoglycemic injury. Stroke 1997;28(3): 584–587.
23. Aoki T, Sato T, Hasegawa K, Ishizaki R, Saiki M. Reversible hyperintensity lesion on diffusion-weighted MRI in hypoglycemic coma. Neurology 2004;63(2): 392–393.
24. Hasegawa Y, Formato JE, Latour LL, et al. Severe transient hypoglycemia causes reversible change in the apparent diffusion coefficient of water. Stroke 1996;27(9):1648–1655; discussion 1655–1656.
25. Huang BY, Castillo M. Hypoxic-ischemic brain injury: imaging findings from birth to adulthood. RadioGraphics 2008;28(2):417–439.
26. Kjos BO, Brant-Zawadzki M, Young RG. Early CT findings of global central nervous system hypoperfusion. AJR Am J Roentgenol 1983;141(6): 1227–1232.
27. Bird CR, Drayer BP, Gilles FH. Pathophysiology of "reverse" edema in global cerebral ischemia. AJNR Am J Neuroradiol 1989;10(1):95–98.
28. Valanne L, Ketonen L, Majander A, Suomalainen A, Pihko H. Neuroradiologic findings in children with mitochondrial disorders. AJNR Am J Neuroradiol 1998;19(2): 369–377.
29. Detre JA, Wang ZY, Bogdan AR, et al. Regional variation in brain lactate in Leigh syndrome by localized 1H magnetic resonance spectroscopy. Ann Neurol 1991;29(2): 218–221.
30. King AD, Walshe JM, Kendall BE, et al. Cranial MR imaging in Wilson's disease. AJR Am J Roentgenol 1996;167(6): 1579–1584.
31. Sener RN. Diffusion MR imaging changes associated with Wilson disease. AJNR Am J Neuroradiol 2003;24(5): 965–967.
32. Kishibayashi J, Segawa F, Kamada K, Sunohara N. Study of diffusion weighted magnetic resonance imaging in Wilson's disease [in Japanese]. Rinsho Shinkeigaku 1993;33 (10):1086–1089.
33. Lampl C, Yazdi K. Central pontine myelinolysis. Eur Neurol 2002;47(1):3–10.
34. Adams RD, Victor M, Mancall EL. Central pontine myelinolysis: a hitherto undescribed disease occurring in alcoholic and malnourished patients. AMA Arch Neurol Psychiatry 1959;81(2):154–172.
35. Miller GM, Baker HL Jr, Okazaki H, Whisnant JP. Central pontine myelinolysis and its imitators: MR findings. Radiology 1988;168(3):795–802.
36. Ogershok PR, Rahman A, Nestor S, Brick J. Wernicke encephalopathy in nonalcoholic patients. Am J Med Sci 2002;323(2):107–111.
37. Zuccoli G, Gallucci M, Capellades J, et al. Wernicke encephalopathy: MR findings at clinical presentation in twenty-six alcoholic and nonalcoholic patients. AJNR Am J Neuroradiol 2007;28(7):1328–1331.
38. Hayflick SJ, Westaway SK, Levinson B, et al. Genetic, clinical, and radiographic delineation of Hallervorden-Spatz syndrome. N Engl J Med 2003;348(1): 33–40.

39. Zhou B, Westaway SK, Levinson B, Johnson MA, Gitschier J, Hayflick SJ. A novel pantothenate kinase gene (PANK2) is defective in Hallervorden-Spatz syndrome. Nat Genet 2001;28(4):345–349.
40. Savoiardo M, Halliday WC, Nardocci N, et al. Hallervorden-Spatz disease: MR and pathologic findings. AJNR Am J Neuroradiol 1993;14(1): 155–162.
41. Kretzschmar HA, Ironside JW, DeArmond SJ, Tateishi J. Diagnostic criteria for sporadic Creutzfeldt-Jakob disease. Arch Neurol 1996;53(9):913–920.
42. Steinhoff BJ, Räcker S, Herrendorf G, et al. Accuracy and reliability of periodic sharp wave complexes in Creutzfeldt-Jakob disease. Arch Neurol 1996;53(2):162–166.
43. Zerr I, Bodemer M, Gefeller O, et al. Detection of 14-3-3 protein in the cerebrospinal fluid supports the diagnosis of Creutzfeldt-Jakob disease. Ann Neurol 1998;43(1):32–40.
44. Kandiah N, Tan K, Pan AB, et al. Creutzfeldt-Jakob disease: which diffusion-weighted imaging abnormality is associated with periodic EEG complexes? J Neurol 2008;255 (9):1411–1414.
45. Zeidler M, Sellar RJ, Collie DA, et al. The pulvinar sign on magnetic resonance imaging in variant Creutzfeldt-Jakob disease. Lancet 2000;355(9213): 1412–1418. [Published correction appears in Lancet 2000;356(9224):170.]
46. Tschampa HJ, Mürtz P, Flacke S, Paus S, Schild HH, Urbach H. Thalamic involvement in sporadic Creutzfeldt-Jakob disease: a diffusion-weighted MR imaging study. AJNR Am J Neuroradiol 2003;24(5): 908–915.
47. Avrahami E, Cohn DF, Feibel M, Tadmor R. MRI demonstration and CT correlation of the brain in patients with idiopathic intracerebral calcification. J Neurol 1994;241 (6):381–384.
48. Smith AB, Smirniotopoulos JG, Rushing EJ, Goldstein SJ. Bilateral thalamic lesions. AJR Am J Roentgenol 2009;192 (2):W53–W62.
49. Spearman MP, Jungreis CA, Wehner JJ, Gerszten PC, Welch WC. Endovascular thrombolysis in deep cerebral venous thrombosis. AJNR Am J Neuroradiol 1997;18(3): 502–506.
50. Lim CC. Magnetic resonance imaging findings in bilateral basal ganglia lesions. Ann Acad Med Singapore 2009;38 (9):795–798.
51. Forbes KP, Pipe JG, Heiserman JE. Evidence for cytotoxic edema in the pathogenesis of cerebral venous infarction. AJNR Am J Neuroradiol 2001;22(3): 450–455.
52. Crawford SC, Digre KB, Palmer CA, Bell DA, Osborn AG. Thrombosis of the deep venous drainage of the brain in adults: analysis of seven cases with review of the literature. Arch Neurol 1995;52(11): 1101–1108.
53. Castaigne P, Lhermitte F, Buge A, Escourolle R, Hauw JJ, Lyon-Caen O. Paramedian thalamic and midbrain infarcts: clinical and neuropathological study. Ann Neurol 1981;10(2):127–148.
54. Kostanian V, Cramer SC. Artery of Percheron thrombolysis. AJNR Am J Neuroradiol 2007;28(5): 870–871.
55. Percheron G. The anatomy of the arterial supply of the human thalamus and its use for the interpretation of the thalamic vascular pathology. Z Neurol 1973;205(1):1–13.
56. Lasjaunias P, Berenstein A, Brugge KGT, eds. Surgical neuroangiography. 2nd ed. Vol 1. Berlin, Germany: Springer-Verlag, 2000;526–562.
57. Matheus MG, Castillo M. Imaging of acute bilateral paramedian thalamic and mesencephalic infarcts. AJNR Am J Neuroradiol 2003;24(10):2005–2008.
58. Sakane T, Takeno M, Suzuki N, Inaba G. Behçet's disease. N Engl J Med 1999;341(17):1284–1291.
59. Akman-Demir G, Serdaroglu P, Tasçi B. Clinical patterns of neurological involvement in Behçet's disease: evaluation of 200 patients. The Neuro-Behçet Study Group. Brain 1999;122(pt 11):2171–2182.
60. Hadfield MG, Aydin F, Lippman HR, Sanders KM. Neuro-Behçet's disease. Clin Neuropathol 1997;16(2): 55–60.
61. Rosas H, Wippold FJ 2nd. West Nile virus: case report with MR imaging findings. AJNR Am J Neuroradiol 2003;24 (7):1376–1378.
62. Einsiedel L, Kat E, Ravindran J, Slavotinek J, Gordon DL. MR findings in Murray Valley encephalitis. AJNR Am J Neuroradiol 2003;24(7):1379–1382.
63. Kumar S, Misra UK, Kalita J, Salwani V, Gupta RK, Gujral R. MRI in Japanese encephalitis. Neuroradiology 1997;39 (3):180–184.
64. Prakash M, Kumar S, Gupta RK. Diffusion-weighted MR imaging in Japanese encephalitis. J Comput Assist Tomogr 2004;28(6):756–761.
65. Colombo FA, Vidal JE, Penalva de Oliveira AC, et al. Diagnosis of cerebral toxoplasmosis in AIDS patients in Brazil: importance of molecular and immunological methods using peripheral blood samples. J Clin Microbiol 2005;43 (10):5044–5047.
66. Navia BA, Petito CK, Gold JW, Cho ES, Jordan BD, Price RW. Cerebral toxoplasmosis complicating the acquired immune deficiency syndrome: clinical and neuropathological findings in 27 patients. Ann Neurol 1986;19(3):224–238.
67. Dina TS. Primary central nervous system lymphoma versus toxoplasmosis in AIDS. Radiology 1991;179(3): 823–828.
68. Erdag N, Bhorade RM, Alberico RA, Yousuf NP, Patel MR. Primary lymphoma of the central nervous system: typical and atypical CT and MR imaging appearances. AJR Am J Roentgenol 2001;176(5): 1319–1326.
69. Chang L, Miller BL, McBride D, et al. Brain lesions in patients with AIDS: H-1 MR spectroscopy. Radiology 1995; 197(2):525–531.
70. Smyth EG, Stern K. Tumors of the thalamus: a clinicopathological study. Brain 1938;61(4):339–374.
71. Partlow GD, del Carpio-O'Donovan R, Melanson D, Peters TM. Bilateral thalamic glioma: review of eight cases with personality change and mental deterioration. AJNR Am J Neuroradiol 1992;13(4): 1225–1230.
72. Menon G, Nair S, Krishnamoorthy T, et al. Bilateral thalamic glioma: report of four cases and review of literature. J Pediatr Neurosci 2006;1(2):66–69.
73. Bognanno JR, Edwards MK, Lee TA, Dunn DW, Roos KL, Klatte EC. Cranial MR imaging in neurofibromatosis. AJR Am J Roentgenol 1988;151(2): 381–388.
74. DiPaolo DP, Zimmerman RA, Rorke LB, Zackai EH, Bilaniuk LT, Yachnis AT. Neurofibromatosis type 1: pathologic substrate of high-signal-intensity foci in the brain. Radiology 1995;195(3):721–724.
75. Castillo M, Green C, Kwock L, et al. Proton MR spectroscopy in patients with neurofibromatosis type 1: evaluation of hamartomas and clinical correlation. AJNR Am J Neuroradiol 1995;16(1):141–147.

Differential Diagnosis for Bilateral Abnormalities of the Basal Ganglia and Thalamus

Amogh N. Hegde, MD, FRCR • Suyash Mohan, MD, PDCC • Narayan Lath, MD, FRCR • C. C. Tchoyoson Lim, MMed, FRCR

RadioGraphics 2011; 31:5–30 • **Published online** 10.1148/rg.311105041 • **Content Codes:** MR NR

Page 7
The putamen and globus pallidus are rich in mitochondria, vascular supply, neurotransmitters, and chemical content compared with other areas in the brain, and their high metabolic activity and increased utilization of glucose and oxygen make them vulnerable to metabolic abnormalities and many systemic or generalized disease processes

Page 11
In patients with unexplained coma, determination of blood serum sugar levels can help differentiate this potentially reversible condition from other causes such as hypoxic ischemic encephalopathy (HIE) or acute cerebral infarction

Page 16
Restricted diffusion seen at diffusion-weighted MR imaging is attributed to spongiform neuronal degeneration and is more sensitive than T2-weighted imaging findings in detecting CJD, especially for cortical lesions

Page 19
Simultaneous bilateral involvement of the thalamus and basal ganglia in the appropriate clinical setting should prompt a search for subtle signs of venous thrombosis such as loss of flow void and hyperintense thrombus in the straight sinus, vein of Galen, and internal cerebral veins on conventional MR images

Page 25
Bilaterally symmetric diffuse abnormalities involving the lentiform and caudate nuclei in their entirety typically suggest systemic or metabolic causes, whereas asymmetric, focal, or discrete lesions affecting only part of the basal ganglia tend to indicate involvement by infections or neoplasms.